EMBRY-RIDDLE
Aeronautical University
SCHOLARLY COMMONS

Dissertations and Theses

12-2017

Aerodynamic and Performance Analysis of a Morphing Helicopter Rotor System

Vinay Gopal Krishnan

Follow this and additional works at: https://commons.erau.edu/edt

Part of the Aerospace Engineering Commons

Scholarly Commons Citation

Krishnan, Vinay Gopal, "Aerodynamic and Performance Analysis of a Morphing Helicopter Rotor System" (2017). *Dissertations and Theses*. 369.
https://commons.erau.edu/edt/369

This Thesis - Open Access is brought to you for free and open access by Scholarly Commons. It has been accepted for inclusion in Dissertations and Theses by an authorized administrator of Scholarly Commons. For more information, please contact commons@erau.edu.

AERODYNAMIC AND PERFORMANCE ANALYSIS OF A MORPHING HELICOPTER ROTOR SYSTEM

A Thesis

Submitted to the Faculty

of

Embry-Riddle Aeronautical University

by

Vinay Gopal Krishnan

In Partial Fulfillment of the

Requirements for the Degree

of

Master of Science in Aerospace Engineering

December 2017

Embry-Riddle Aeronautical University

Daytona Beach, Florida

AERODYNAMIC AND PERFORMANCE ANALYSIS OF A MORPHING HELICOPTER ROTOR SYSTEM

by

Vinay Gopal Krishnan

A Thesis prepared under the direction of the candidate's committee chairman, Dr. J Gordon Leishman, Department of Aerospace Engineering, and has been approved by the members of the thesis committee. It was submitted to the School of Graduate Studies and Research and was accepted in partial fulfillment of the requirements for the degree of Master of Science in Aerospace Engineering.

THESIS COMMITTEE

Chairman, Dr. J Gordon Leishman

Member, Dr. Tasos Lyrintzis

Member, Dr. John Ekaterinaris

Graduate Program Coordinator, Dr. Magdy Attia — 12.7.2017 Date

Dean of College of Engineering, Dr. Maj Mirmirani — 12/7/2017 Date

Vice Chancellor, Academic Support, Dr. Christopher Grant — 12/7/17 Date

ACKNOWLEDGMENTS

To begin with, I would like to thank my advisor Dr. J Gordon Leishman for all the help and support that he provided. More than all, he has shown extreme patience and provided valuable guidance during moments of confusion. I am also grateful to Dr. Lyrintzis and Dr. Ekaterinaris for the help they have provided me. I'd like to thank my parents for always being supportive of my passion and encouraging me. Lastly, I'd like to thank Stanrich, Yogesh, Paolo and every other friend who has helped me in the completion of this thesis.

TABLE OF CONTENTS

Page

LIST OF TABLES vi

LIST OF FIGURES vii

ABBREVIATIONS x

NOMENCLATURE xi

ABSTRACT xiii

1 Introduction 1
- 1.1 Literature Review 6
- 1.2 Objectives of this Thesis 13
- 1.3 Summary of Thesis 13

2 Methodology 15
- 2.1 Basic Method 16
  - 2.1.1 Inflow Distribution 19
  - 2.1.2 Rotor Thrust, Power and Drag 21
  - 2.1.3 Blade Flapping 24
  - 2.1.4 Airfoil Characteristics 26
- 2.2 Rotor Trim 27

3 Results and Discussion 33
- 3.1 Validation 33
- 3.2 Blade Morphing: Varying Single Parameters 37
  - 3.2.1 Blade Twist Variations 38
  - 3.2.2 Rotor Radius Variations 42
  - 3.2.3 Rotor Speed (rpm) Variations 45
  - 3.2.4 Blade Chord Variations 46
- 3.3 Morphing Variations with Airspeed 47
  - 3.3.1 Individual Effects 47
  - 3.3.2 Morphing Two Effects Together 49
  - 3.3.3 Morphing Three Effects Together 50

4 Conclusion and Recommendations for Future Work 71
- 4.1 Conclusions 71
- 4.2 Recommendations for Future Work 74

A Appendix: Main MATLAB Code 81

B Flapping Function Code 92

LIST OF TABLES

Table Page

3.1 Parameters used for the validation. 33

LIST OF FIGURES

Figure		Page
1.1	Igor Sikorsky's VS-300 in 1940 [Ref. 1]	1
1.2	Sikorsky's UH-60 Black Hawk in 2004 [Ref. 2]	2
1.3	Complications related to helicopter aerodynamics including stall, compressibility etc. [Ref. 3]	3
1.4	Futuristic vision of a helicopter	4
1.5	Airfoil tab controlled by SMA's [Ref. 10]	5
2.1	Discretization into blade elements along the blade span and showing the relative flow velocities.	17
2.2	Drag vs angle of attack curve for the SC1095 showing the polynomial second-order curve fit and equation used.	19
2.3	Longitudinal and lateral forms of the linear inflow model.	21
2.4	Compressibility and reverse flow regions on the rotor disk.	26
2.5	Forces on a helicopter in forward flight.	28
2.6	Forces acting on a helicopter in forward flight.	30
3.1	Lift distribution for different linear twists.	34
3.2	Thrust distribution for different linear twists.	35
3.3	Inflow distribution for different linear twists.	36
3.4	Collective pitch variations with thrust at hover.	37
3.5	Flapping response for different initial values of β_0.	38
3.6	Flapping response at airspeed of 60 knots before trimming.	39
3.7	Flapping response at 60 knots after being trimmed to meet propulsive requirement with $\alpha_{TPP} = 4.5^\circ$.	40
3.8	Comparison of control input angles between flight test and current method.	41
3.9	Power comparison between current method and test flight for the UH-60 (Weight = 16,000 lb and altitude = 5,200 ft).	42

Figure Page

3.10 Lift-to-drag ratio comparison between current method and test flight for the UH-60. 43

3.11 Power comparison for variable radius between the present method and [Ref. 32] (W = 18,000 lb). 44

3.12 Power comparison for variable RPM between the present method and [Ref. 32] (W = 18,400 lb). 45

3.13 Blade twist effect on power and variation from the baseline case. 51

3.14 Twist effect on rotor drag and variation from the baseline case. 52

3.15 Twist effect on L/D and variation from the baseline case. 53

3.16 Total thrust (C_{TMR}) variation with twist. 54

3.17 Power variation with rotor radius and airspeed. 55

3.18 L/D variation with rotor radius and airspeed. 56

3.19 Rotor drag variation with rotor radius and airspeed. 57

3.20 Total Thrust (C_{TMR}) variation with rotor radius and airspeed. 58

3.21 Power variation with rotor rpm. 59

3.22 L/D variation with rotor rpm. 60

3.23 Rotor drag variation with rotor rpm. 61

3.24 Total Thrust (C_{TMR}) variation with rotor rpm. 62

3.25 Power variation with chord. 62

3.26 Rotor drag variation with chord. 63

3.27 L/D variation with chord. 63

3.28 Total Thrust (C_{TMR}) variation with chord. 64

3.29 Power comparison for a single morphing effect. 65

3.30 L/D comparison for a single morphing effect. 65

3.31 Rotor Drag comparison for a single morphing effect. 66

3.32 Total thrust (C_{TMR}) comparison for a single morphing effect. 66

3.33 Power comparison for two morphing effects. 67

3.34 L/D comparison for two morphing effects. 67

3.35 Rotor drag comparison for two morphing effects. 68

Figure Page

3.36 Total thrust (C_{TMR}) comparison for two morphing effects. 68

3.37 Power comparison for all three morphing effects. 69

3.38 L/D comparison for all three morphing effects. 69

3.39 Rotor Drag comparison for all three morphing effects. 70

3.40 Total Thrust (C_{TMR}) comparison for all three morphing effects. 70

ABBREVIATIONS

AHS	American Helicopter Society
AoA	Angle of Attack
BET	Blade Element Theory
CFD	Computational Fluid Dynamics
CVF	Curvilinear Fiber Composites
DEAP	Dielectric Polymer
DL	Disk Loading
NASA	National Aeronautics and Space Association
PZT	Piezo-electric Actuators
SMA	Shape Memory Alloy
TPP	Tip Path Plane
UMARC	University of Maryland Advanced Rotor Code

NOMENCLATURE

c	Blade chord
C_H	Main rotor drag
C_l	Coefficient of lift
C_{l_α}	Lift curve slope
C_d	Coefficient of drag
C_P	Coefficient of power
$C_{P_{MR}}$	Coefficient of power of main rotor
C_{p_i}	Induced power coefficient
C_{p_0}	Profile power coefficient
C_{p_p}	Parasitic power coefficient
e	Hinge offset
f	Equivalent drag area of the airframe
I_b	Mass moment of inertia about flapping hinge
L/D	Lift to drag ratio
$\bar{M}_\beta$	Aerodynamic moment about the flapping hinge
N_b	Number of blades
R	Blade radius
U_P	Inflow perpendicular to rotor disk
U_T	In-plane velocity to rotor disk
V_{TIP}	Blade tip speed
W	Gross weight of helicopter

GREEK ALPHABETS

α	Angle of attack
α_{TPP}	Angle of attack of Tip Path Plane
$\dot{\beta}$	Blade flapping velocity
β_{1c}	Longitudinal flapping angle
β_{1s}	Lateral flapping angle
γ	Lock number
θ	Blade pitch
θ_{TW}	Blade linear twist rate
θ_{1c}	Lateral cyclic
θ_{1s}	Longitudinal cyclic
λ	Nondimensional inflow
λ_0	Average nondimensional Inflow
μ	Advance ratio

ν_β	Flap frequency
ρ	Density of air
σ	Rotor solidity
χ	Wake skew angle
ϕ	Inflow angle
ψ	Blade azimuth angle

ABSTRACT

Gopal Krishnan, Vinay MSAE, Embry-Riddle Aeronautical University, December 2017.

Aerodynamic and Performance Analysis of a Morphing Helicopter Rotor System .

The purpose of this study was to investigate the effect of rotor morphing, specifically variable rotor speed and variable blade twist, on various parameters such as the distribution of angle of attack, lift, power, thrust and/or other metrics describing the performance of a helicopter rotor. A MATLAB based blade element theory model was developed and executed for different flight conditions. The model was validated against the flight test data of a UH-60. Effects on power, lift to drag ratio and rotor drag from variations in blade twist, rotor speed, rotor radius and blade chord was analyzed. Morphing cases were applied as linear functions of airspeed. Linearly varying rotor speed provides the most benefits at higher airspeeds for individual morphing cases, while linearly varying twist with airspeed provided the most rotor drag reduction. For cases where two elements of morphing were used, varying blade twist and radius provided the most benefits at higher airspeeds, while also providing the most drag reductions in all cases. When morphing twist, radius and rotor speed simultaneously, the power reductions obtained were the most significant, while also having substantial decreases in rotor drag. A maximum power reduction of about 20% was obtained at higher airspeeds with the judicious application of all elements of blade and rotor morphing.

1. Introduction

The quest for vertical flight goes back over a century, but the vision of a helicopter that was a practical an useful form of aircraft took many years to realize even after airplanes were flying successfully. Juan de la Cierva and Igor Sikorsky were among many of the early pioneers who tried their hand at developing rotating wing aircraft. But because of limitations with engine power, airframe weight, rotor vibrations, etc., amongst other problems, their efforts did not at first lead to practical concepts. Most early helicopters hopped off the ground for a few seconds more than flew, leading to the nickname of "hoppers."

Figure 1.1: Igor Sikorsky's VS-300 in 1940 [Ref. 1]

Comparing those early attempts at vertical flight to the capabilities of modern helicopter, it can be seen that there have been many technological developments. These developments easily become apparent when comparing the VS-300 (Fig. 1.1) to the UH-60 Black Hawk (Fig. 1.2). The modern helicopter is indeed a triumph of aeronautical engineering, the aircraft being able to hover, fly forward, sidewards or backwards, all at the whim of the pilot. However, while there have been many advancements, helicopters still continue to experience several aeromechanical problems that limit their flight capabilities. The main limitations of helicopters are relatively low maximum forward flight speeds (typically less than 150 knots), high vibration levels, and obtrusive noise levels under many flight conditions. These issues are summarized in Fig. 1.3.

Figure 1.2: Sikorsky's UH-60 Black Hawk in 2004 [Ref. 2]

Specific aerodynamic concerns related to a helicopter in forward flight include blade stall on the retreating side and compressibility issues near the advancing blade tips. While

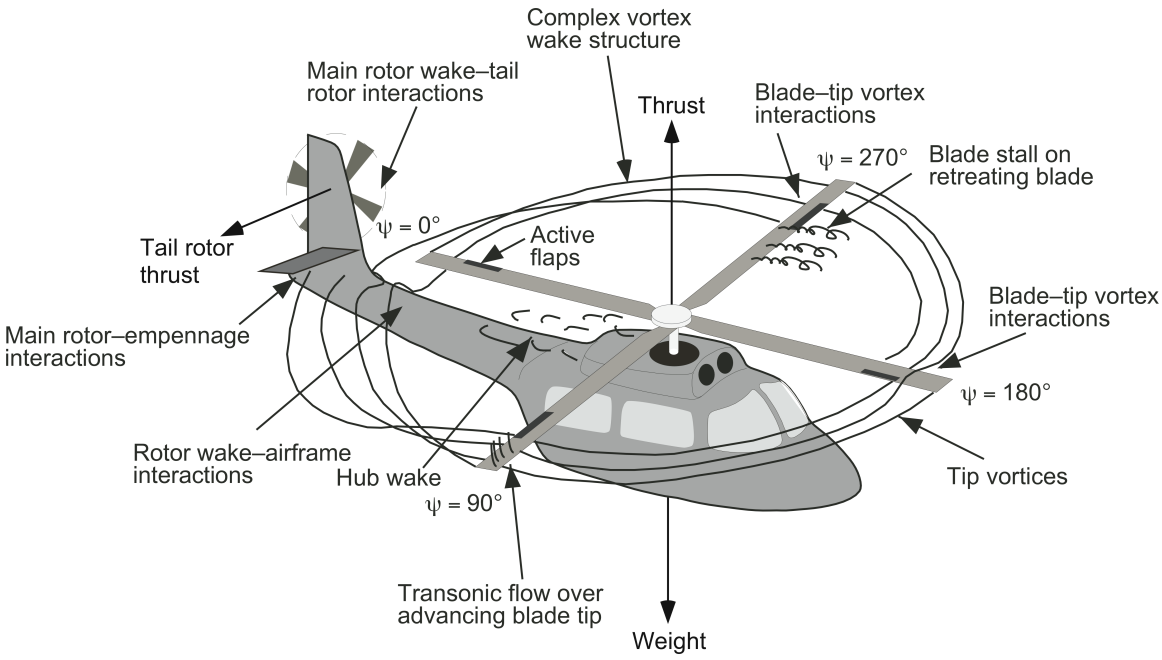

Figure 1.3: Complications related to helicopter aerodynamics including stall, compressibility etc. [Ref. 3]

forward speed can be increased by adding more power, the associated increase in empty weight can decrease useful load, i.e., a reduction of payload and/or fuel. Therefore, other means become necessary to further push the boundaries of helicopters, namely airfoil optimization, swept tips and streamlining the fuselage.

Figure 1.4 shows a summary of just some the ideas that have been put forth to extend the capabilities of a conventional helicopter. The ideas include advanced blade shapes and blade tips, morphing blades, lift compounding, propulsive compounding, elimination of the tail rotor in leu of some other type of system, etc. However, implementation of all these technologies, especially at the same time, would be extremely difficult if not impractical.

Each system shown in Fig. 1.4 requires its own supporting systems, which would not only increase the total empty weight but also drive up significantly the cost of the helicopter.

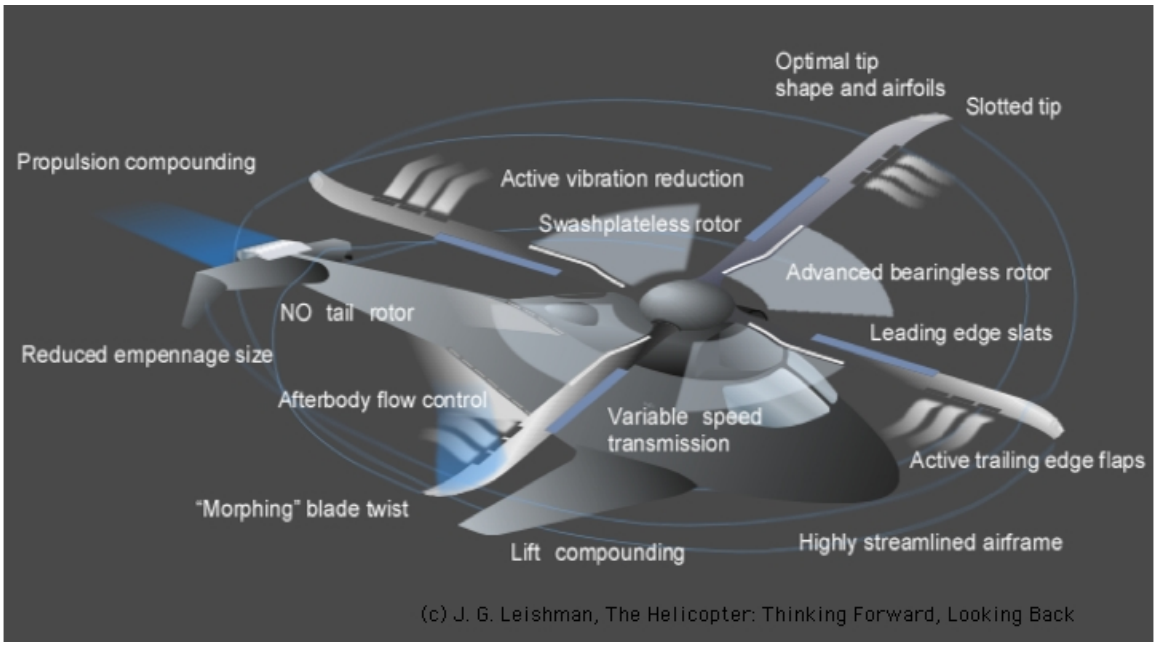

Figure 1.4: Futuristic vision of a helicopter

That being said, some of the technologies shown in Fig. 1.4 continue to be researched, and indeed some may be eventually implemented in modern helicopters. For example, nearly all modern helicopters use swept tips to delay the onset of compressibility. Improvements in airfoils have been tremendous, modern day helicopters using special cambered airfoils that are optimized to the blade stations. Other research has been conducted to optimize airfoils without geometric constraints [Ref. 4].

Most recently novel means at overcoming these barrier problems have been considered, including "morphing," for example, active blade twist, rotor radius variations, etc. Such concepts may even be practical with the used of smart materials, which can change their

shape in response to an external stimuli, e.g., electric current, heat, etc. There are many types of shape changing materials with the elements that influence them being different. For example, piezoelectric actuators (PZT) and dielectric polymers (DEAP) are responsive to electricity, while shape memory alloys (SMA) react to heat. Some common materials used to alter the shapes of airfoils and wings are PZT's and SMA's. PZT's have many applications ranging from biomedical [Ref. 5] to aerospace [Ref. 6]. Similarly SMA's have a wide range of applications varying from dental wires [Ref. 7], blood pumps [Ref. 8] to airfoils [Ref. 9]. PZT's and SMA's are the most commonly used smart materials in the aerospace industry. Figure 1.5 shows an example of a tab on a blade section that is proposed to be controlled by SMA's.

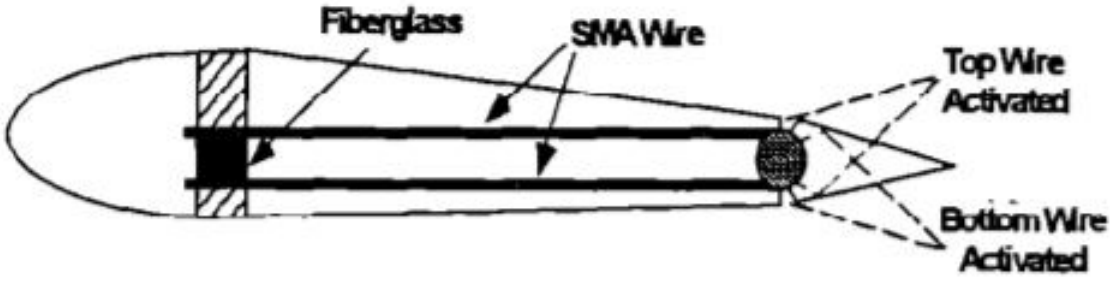

Figure 1.5: Airfoil tab controlled by SMA's [Ref. 10]

Changing the shape of rotor parameters during flight (e.g., rotor radius, blade chord, blade twist, etc.) might also help extend the boundaries of helicopter flight, however it is recognized that this is a more ambitious approach. Therefore, this thesis examines the impact of morphing on a helicopter rotor system, but from a purely aerodynamic and performance point of view. Structural deformations and aeroelastic effects etc. are ignored,

the reason being that unless a "morphing" rotor can be well justified from an aerodynamic and performance perspective then it is unlikely to be justified from any other perspective. Only the main rotor, which is the primary mover, is taken in consideration, and both hover and forward flight regimes are examined.

1.1 Literature Review

There has been considerable work done in three fields related to the potential of making a morphing rotor system practical, namely structures, controls, as well as aerodynamics and performance. This thesis examines the aerodynamic and performance aspects of a morphing rotor, so a thorough literature review of prior work was conducted mainly in this area.

From a flight controls perspective, a variable sweep and span morphing Unmanned Aerial Vehicle (UAV) was analyzed by using *Surfaces* (a vortex lattice method software) and *Simulink* by Prabhakar [Ref. 11]. Haibo et al. [Ref. 12] conducted research related to a variable rotor speed control for a helicopter/engine system. Similarly, the National Aeronautics and Space Administration (NASA) [Ref. 13] conducted research on a control shifting algorithm for a variable rotor speed system. Belmonte et al. [Ref. 14] performed an analysis on disturbance rejection controls for a small–scale helicopter rotor with variable speed rotor.

There has been several advancements related to morphing wings and airfoils from a structural point of view. After the development of smart materials such as SMA's, stack PZT, etc., research has been done into altering the camber, twist and even the span of

a wing. Woods et al. [Ref. 15] used curvilinear fiber composites (CVF) on the skin to produce an airfoil for a rotor system that can change its camber. Han and Smith [Ref. 16] conducted research related to aeroelastic effects of a variable speed rotor in forward flight. The 2/revolution lagwise root bending moment was found to increase significantly while flapping motion contributed significantly to the lagwise loads. It was concluded that increasing blade lag damping could significantly reduce the maximum transient rotor torque.

Chen and Chopra [Ref. 17] conducted wind tunnel testing of a smart rotor with blade twist control. $1/8$ th scaled bearingless rotor model was tested in the University of Maryland's Glenn L. Martin Wind Tunnel. The blade twist was induced using PZT actuators. The model was tested at three different rotor speeds and the rotor was trimmed to a specified flight condition before being tested with active twist control. The authors observed reductions in vibratory rotor torque and moment,s while an increase in hub loads was also noticed. The authors state that further work is needed to be done to compare the data obtained with UMARC (University of Maryland Advanced Rotor Code) to refine the rotor design for improved performance.

There has been similar work done in controlling vibrations in wind turbines using variable rotor speed by Staino and Basu [Ref. 18]. Han et al. [Ref. 19] studied transient loads that occur in a variable speed rotor. Prahlad and Chopra [Ref. 20] designed a variable twist rotor blade for a tilt rotor using SMA actuators. Ajaj et al. [Ref. 21] performed a feasibility study on twist morphing using variable cross section spar. Gandhi et al. [Ref. 22] conducted research into a "conformable" rotor airfoil using PZT's [Ref. 23].

From an aerodynamic point of view, there have been various research activities conducted using morphing wings and optimizing airfoils undergoing morphing. A variable span wing was analyzed for drag reduction by Mestrinho et al. [Ref. 24]. The wing was experimentally tested, while the aerodynamic coefficients were computed using a mathematical model. A traditional aileron system could not be used, so roll was achieved by using differences in wing semi-span. The results showed significant decrease in drag at higher flight speeds and roll rate performance was similar to that with a traditional aileron. Several factors that would be crucial to flight are flutter, gust response etc., however, none of these concepts were actually analyzed. These phenomena would have significant effect on flight performance because the impact of ailerons were obtained by adjusting wing span and not with ailerons.

Similar research related to morphing wings for small UAV's have been conducted by Secanell et al. [Ref. 25]. The purpose of this study was to alter the airfoil during take-off, landing, cruise, loiter and even at the onset of wing stall. The analysis was conducted using CFD with Spalart-Allmaras turbulence model and a sequential quadratic programming algorithm. From the results, it was concluded that the airfoils for all flight conditions except stall shared one common feature, namely their thickness distribution. The airfoil needed at stall had a higher leading edge thickness, while the camber was different for all other cases. The power required for flight decreased but the decrement was small for the given flight conditions. Each case was tested at a different flight condition. Hence, it was concluded that the power savings could be more significant for other flight regimes and even in sustained low-speed maneuvers. Two factors ignored in this paper were the additional

weight because of the mechanisms required for morphing, and only the aerodynamics of the airfoil were considered not the entire aircraft, as compared to that done by Mestrinho et al. although they only considered variable span. Miste and Benini [Ref. 26] conducted a performance comparison between continuously variable and fixed ratio gearbox.

When it comes to helicopters, work related to optimizing airfoils for helicopter blades had been undertaken by Fusi and Congedo [Ref. 4]. The two objectives were to maximize the lift to drag ratio, C_l/C_d, on the advancing side of the rotor and the ratio $C_l^{\frac{3}{2}}/C_d$ on the retreating side, while also designing an airfoil that was insensitive to gusts, etc. The evaluation was conducted using Computational Fluid Dynamics (CFD) using a MSES solver coupled with a Euler/integral boundary layer code. MSES is a suite of programs used to design and analyze airfoils [Ref. 27]. Both angle of attack and Mach number were considered as variables on the advancing side, while only angle of attack was considered as a variable on the retreating side. Two different airfoils were obtained based on the defined conditions, an assumption being that there are no geometrical constraints for the morphing shape. The airfoil that was optimized for the advancing side had its maximum camber located farther from the leading edge than the airfoil optimized for the retreating side. Hence, the optimization results were two decoupled optimizations at two different operating conditions. From the results, it could be inferred that morphing an airfoil does give some benefit from an aerodynamic point of view as long as there are no constraints on the geometric shape of the airfoil. However, this study ignored the requirements for rotor trim as well as lift constraints on the airfoil, which are essential to analyze a rotor system in forward flight.

NASA and Sikorsky have conducted wind tunnel test on a variable diameter tilt rotor [Ref. 28]. Although a wind tunnel test was conducted, the variable diameter rotor was never put into production. The benefits of a VDTR concept include better hovering efficiency (with the blades extended like helicopter) and better propulsive efficiency in forward flight (with the blades retracted like a propeller). Khoshlajeh and Gandhi [Ref. 29] conducted research into using extendable chord rotors for performance improvement. Mistry and Gandhi [Ref. 30] performed analysis on variable rotor radius and rotor speed. With rotor speed variation only, power reductions of up to 14% was obtained. On combining radius and rotor speed variations, the power reductions were found to be significantly higher than with radius or speed variation alone. It was also concluded that weight and altitude play a significant effect on the performance gains that could be obtained. Porter et al. [Ref. 31] have conducted an experimental analysis on variable collective pitch rotor, the outcomes showing that variable collective pitch rotors have better performance over fixed pitch rotors.

Although there are several papers related to morphing rotor systems, only two papers focus on representing the aerodynamic and performance effects on a morphing rotor system. Chopra [Ref. 32] examined the aeromechanics of an actively morphing rotor system, which includes the interactions between the aerodynamic and structural components. Two parameters considered were variable rotor speed and variable blade radius. The baseline helicopter used was the UH-60 Black Hawk. The program used for this analysis was University of Maryland Advanced Rotor Code (UMARC). For the analysis of variable rotor speed, the paper states that "at a mission weight of 18,400 lb, a maximum power reduction of 10% can be achieved at moderate cruise speeds. At 14,000 lb, which corresponds to

the empty weight of the UH-60, up to 20% power reduction is achievable." The authors concluded that the effects of variable rotor speed were dependent on the operating weight and flight conditions. In regard to variable rotor radius, it was shown to reduce power at higher airspeeds. The authors state "for a 16,000 lb helicopter, up to 180 hp reduction can be achieved at 170 knots with just a 5% reduction in radius. This would approximately be equal to a 5% reduction in total power." It was also found that the benefits reduce as thrust increases but at more conservative mission profiles there are potential fuel savings of between 20 and 60 lb/hr, which are modest but significant.

Barakos et al. [Ref. 33] have conducted an aerodynamic as well as structural analysis for a rotor with variable rotor speed and blade twist. Two models were used, a semi-empirical aerodynamic model and CFD. The blade used was selected to mimic the UH-60A. The model used for the induced velocity over the rotor was the Pitt-Peters dynamic inflow model. The CFD model used was the Reynolds-Averaged Navier-Stokes (RANS) method with the $k-\omega$ turbulence closure model. Four different aircraft weight coefficients were considered and the corresponding power curves for flight were obtained. Rotor power reductions of 7–17% were noticed while decreasing speed between 5–15%. Reducing the rotor speed too much at higher airspeeds led to a larger stall area. As twist changed from -16° to 0°, power increased from 0.5–10% of the initial required power, although for advance ratios near 0.3 the power decreased. Combining blade twist variations with rotor speed variation resulted in a more significant decrease in power required. The authors also stated that variable twist could also possibly reduce the blade loads introduced by varying rotor speed. A conclusion was drawn that large decrease in rotor speed is to be

avoided because it then has a negative effect on performance, namely increase in power requirements. The paper does not mention the procedure used for rotor trim, a fundamental and glaring omission.

Recently, Bell came out with a concept named the "FCX-001" that has morphing blade tips [Ref. 34]. Depending on flight condition, the tips adjust their sweep to optimize flight performance. Sweeping back the rotor blades at higher speeds helps alleviate compressibility effects while having no sweep in hover enables a larger disk area and a lower disk loading and hence a lower power requirement. However, the mechanical methods used to accomplish this type of blade morphing are not yet clear.

From the foregoing discussion, two primary observations can be made. Firstly, morphing wings and helicopters rotors may be possible and may have some performance advantages. Research has been made using smart materials or other mechanisms to alter camber, blade twist and even rotor radii. Although from a structural as well as singular focus (blade twisting alone and variable radius alone), some wind tunnel testing has also been conducted to explore the potential benefits. Advancements in flight controls means that it is possible to design and control morphing wings or blades. Secondly, most of the research related to morphing rotors has been done in the field of structures or controls. There seems to be a lack of basic research related to the aerodynamics or performance of morphing rotors. Even though there are two papers associated with the aerodynamic and performance aspect i.e., Chopra [Ref. 32] and Barakos et al. [Ref. 33], they are not particularly comprehensive and seem to cover just a few concepts, e.g., just variable speed or rotor radius, etc.

1.2 Objectives of this Thesis

This thesis titled "Aerodynamic and Performance Analysis of a Morphing Helicopter Rotor System" has the following primary objectives:

1. Use a blade element based rotor model to examine the possible performance benefits that could be obtained by the use blade "morphing," either as individual effects or using combinations of effects.

2. Conduct parametric study of "morphing" effects such as by varying blade twist, rotor speed, rotor radius and blade chord to determine their effects on power requirements for flight, the effects on rotor and vehicle lift to drag ratio, and other factors that may enhance or limit the operational capabilities of the rotor system.

1.3 Summary of Thesis

Chapter 1 of this thesis contains a discussion of the motivation for this work as well as the previous work related to the field of blade and/or rotor morphing. Discussed in Chapter 2 is the methodology used for this thesis. The methodology chapter discusses the implementation of the blade element theory in MATLAB and its validation using flight test data of the UH-60. Chapter 3 discusses the results that were obtained. The effects of varying blade twist, rotor rpm, rotor radius and blade chord on power, lift to drag ratio, rotor drag and thrust are examined. First, individual morphing methods (e.g., blade twist only, rotor speed only etc.) are considered, then combinations of methods are examined.

Chapter 4 gives summary of conclusions obtained, as well as the recommendations made for future research.

2. Methodology

The blade element theory (BET) was used as a means of analyzing the aerodynamics of a morphing helicopter rotor. The BET, with certain assumptions and simplifications, provides an estimate of the blade loads in space along the span of the blade, as well as in time around the rotor azimuth. After the elemental values at each blade element have been determined, the overall rotor performance such as thrust and power, and also rotor drag etc., can be obtained by integrating sectional airloads over the blade span and around the azimuth. The outcome is a revolution-by-revolution time-history of the rotor performance, which can also be modulated using blade pitch inputs to trim the rotor to a particular operating state, i.e., thrust and disk orientation.

The BET is a relatively powerful yet simplified theory, which assumes as a basis that each section at the blade behaves as a 2-dimensional airfoil section. This theory does not explicitly account for effects such as highly non-uniform inflow velocities induced by the tip vortices, yet a method known as Prandtl's tip loss function can be used within the theory to represent the 3-dimensional effects that we associated with the rollup of a vortex from the blade tip. The BET generally slightly over-predicts rotor thrust and somewhat under-predicts torque, but the method does provide a good computative tool for relative comparison purposes. Hence, the BET was used as the basis for the results in this thesis, and the coding of the theory was implemented in MATLAB.

2.1 Basic Method

The BET calculates the local coefficients at each blade element such as section lift, thrust, drag, torque, etc. and then integrates these values over the span of the blade and around the azimuth, thereby obtaining the total performance metrics for the rotor. For the spanwise integration, the blade was divided into N discrete blade elements and the aerodynamic effects occurring at each blade element, which is at a distance of y from the hub, are considered. This discretization into blade elements along the blade span and relative flow velocities are shown in Fig. 2.1.

The airloads depend on the angle of attack and the velocity relative to each blade section, the blade element diagram also being shown in Fig. 2.1. The blade pitch is defined in terms of the collective pitch θ_0, lateral cyclic θ_{1c} and longitudinal cyclic θ_{1s} by

$$\theta(y,\psi) = \theta_0 + \theta_{TW} y + \theta_{1c}\cos\psi + \theta_{1s}\sin\psi \tag{2.1}$$

where θ_{TW} is the linear twist rate along the blade and is measured in units of twist angle per rotor radius. The inflow perpendicular to the rotor disk, U_P, is calculated by using

$$U_P = \lambda(y,\psi)\ V_{\text{tip}} + \dot{\beta} y \tag{2.2}$$

where the blade flapping velocity is given by $\dot{\beta} = d\beta(\psi)/dt$ (flapping is considered later) and $\lambda(y,\psi)$ is the non-dimensional inflow distribution, which is also defined later. The in-plane component of velocity, U_T, is given by

$$U_T = \Omega(y + \mu R\ \sin\psi) \tag{2.3}$$

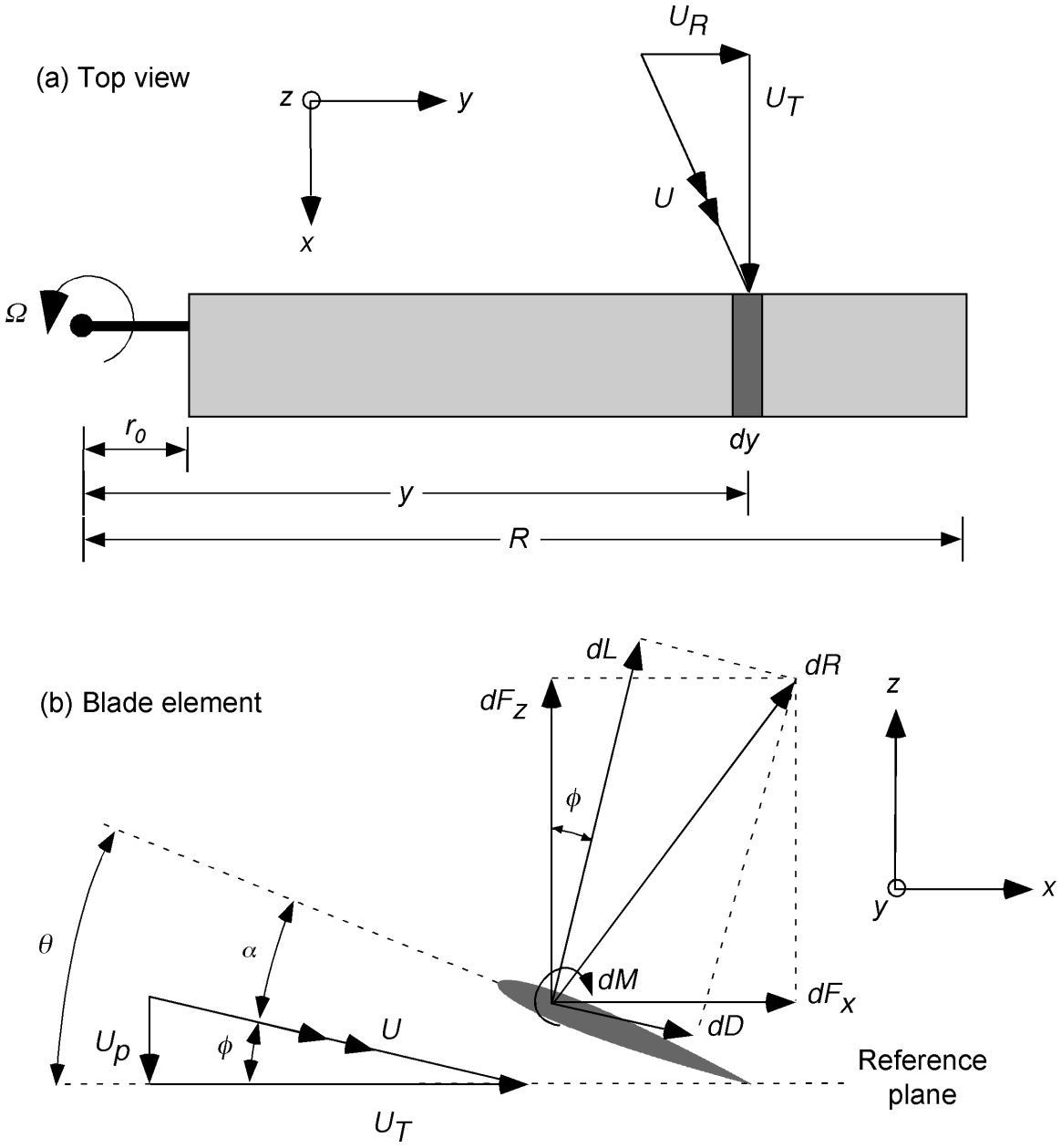

Figure 2.1: Discretization into blade elements along the blade span and showing the relative flow velocities.

which is the sum of the rotational and translational parts. The rotor advance ratio is defined as

$$\mu = \frac{V_\infty \cos(\alpha_{\text{TPP}})}{V_{\text{tip}}} \tag{2.4}$$

where $V_{\text{tip}} = \Omega R$ is the hover tip speed and α_{TPP} is the tip path plane angle of attack.

The inflow angle at each blade element is then given by

$$\phi(y,\psi) = \tan^{-1}\left(\frac{U_P}{U_T}\right) \tag{2.5}$$

and so the aerodynamic angle of attack at the blade section is given by

$$\alpha(y,\psi) = \theta(y,\psi) - \phi(y,\psi) = \theta - \tan^{-1}\left(\frac{U_P}{U_T}\right) \tag{2.6}$$

The local coefficients of lift and drag are then calculated using

$$C_l(y,\psi) = C_{l\alpha}\ (\alpha - \alpha_0) \tag{2.7}$$

where $C_{l\alpha}$ is the lift curve slope of the airfoil. The SC1095 was chosen as it is the airfoil used in the UH-60. . The airfoil characteristics of the SC1095 are obtained from [Ref. 35]. Zero-lift angle ($\alpha_\circ$), is -0.7°. The coefficient of drag below stall is given in terms of constants d_1 and d_2,

$$C_d = C_{d_0} + d_1\ \alpha + d_2\ \alpha^2 \tag{2.8}$$

where d_1 = -0.0002, d_2 = 0.0002 and C_{d_0} = 0.007 for the SC1095. From [Ref. 36], the C_d vs α curve is obtained and plotted in EXCEL as shown in Fig. 2.2 and a polynomial fit of the second order to the curve is added. Comparing Eq. 2.8 with the equation in Fig. 2.2, enables finding the constants, d_1, d_2 and C_{d_0}. Data used from [Ref. 36] to plot Fig. 2.2 is shown in Appendix 2.

The elemental lift and drag forces per element over the span are then obtained from the respective coefficients, i.e.,

$$dL = \frac{1}{2}\ \rho\ U^2\ c\ C_l\ dy \tag{2.9}$$

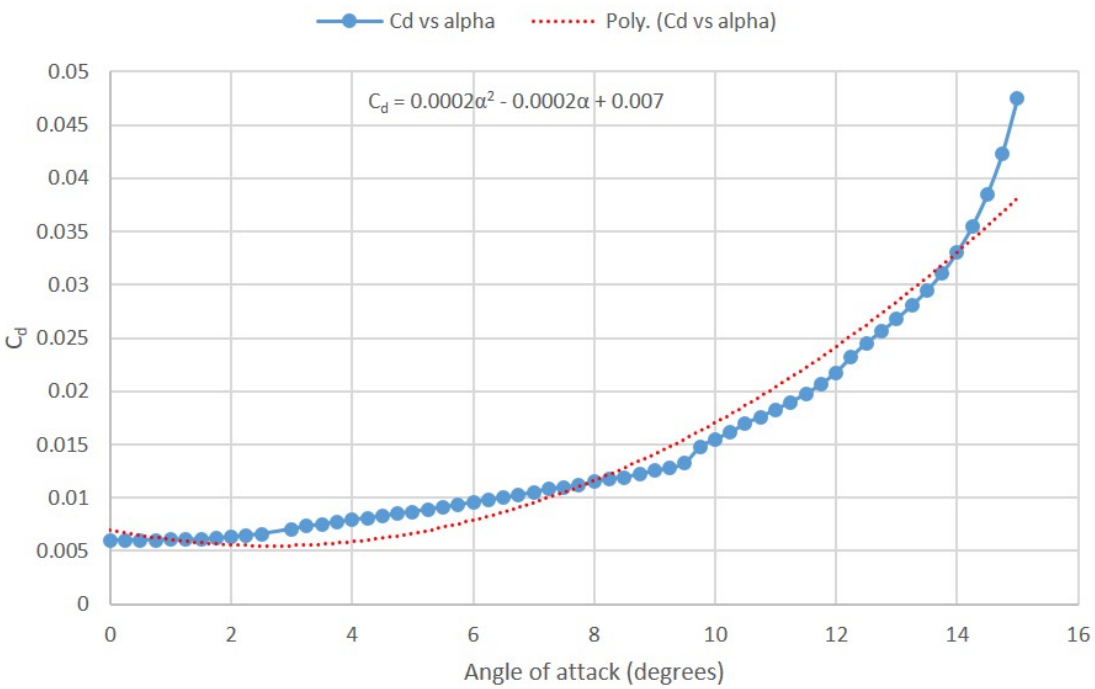

Figure 2.2: Drag vs angle of attack curve for the SC1095 showing the polynomial second-order curve fit and equation used.

and

$$dD = \frac{1}{2}\,\rho\,U^2\,c\,C_d\,dy \tag{2.10}$$

where the resultant velocity is given by $U = \sqrt{U_T^2 + U_P^2}$.

2.1.1 Inflow Distribution

The inflow varies over the span and azimuth and in the present work is described by the linear model Coleman et al. as discussed in [Ref. 3]. The longitudinal and lateral weighting

of the inflow is performed using the coefficients k_x and k_y, and the inflow is calculated by using,

$$\lambda(y,\psi) = \lambda_0\left(1 + k_x\, y\, \cos(\psi) + k_y\, y\, \sin(\psi)\right) \tag{2.11}$$

where λ_0 is the average inflow given according to the simple momentum theory, i.e.,

$$\lambda_\circ = \mu\, \alpha_{\mathrm{TPP}} + \frac{C_T}{2\sqrt{\mu^2 + \lambda_\circ^2}} \tag{2.12}$$

which is solved iteratively as part of the overall solution process for trim. The local inflow is corrected by the Prandtl tip loss factor to account for the effect of tip loss on inflow. Prandtl's tip loss factor is accounted for using the correction factor F, which was calculated iteratively in a sub-iteration using Eqs. 2.13 and 2.14.

$$F = \left(\frac{2}{\pi}\right)\cos^{-1}\left(\exp(-\mathrm{f})\right) \tag{2.13}$$

where f is given by

$$f = \frac{N_b}{2}\left(\frac{R-y}{y\phi}\right) \tag{2.14}$$

An initial value of 1 was taken and F converged to a value between 0.95–0.98. The inflow weighting factors in the Coleman model are given by

$$k_y = 0 \tag{2.15}$$

and

$$k_x = \tan(\chi/2) \tag{2.16}$$

where χ is the wake skew angle which was obtained using

$$\chi = \tan^{-1}(\mu/\lambda_0) \tag{2.17}$$

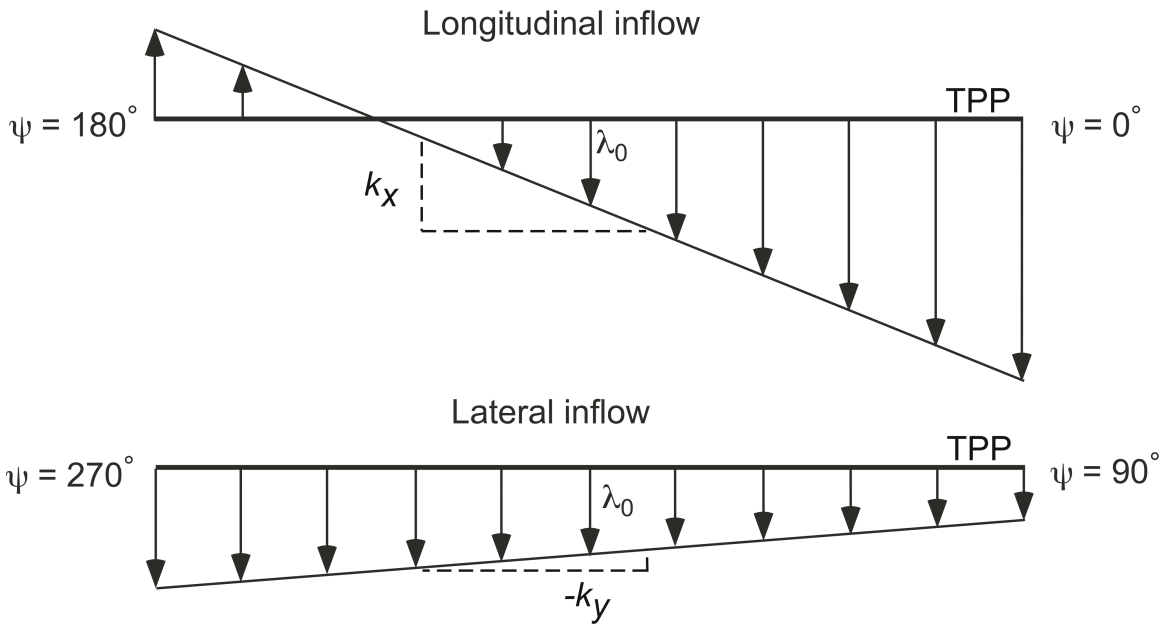

Figure 2.3: Longitudinal and lateral forms of the linear inflow model.

2.1.2 Rotor Thrust, Power and Drag

The rotor thrust increment at each blade element is

$$dT = dL\cos\phi \; - \; dD\sin\phi \tag{2.18}$$

and the integration of rotor thrust over the blade span gives the blade lift, and integration around the azimuth gives the rotor thrust, which in non-dimensional terms is

$$T_{MR} = \frac{N_b}{2\pi}\int_0^{2\pi}\int_0^R dT \; d\psi \tag{2.19}$$

The numerically equivalent incremental thrust at each blade element is

$$\Delta T = \Delta L\cos\phi \; - \; \Delta D\sin\phi \tag{2.20}$$

and in numerical form the thrust is

$$T_{MR} = \frac{N_b}{4\pi} \sum_{j=2}^{M} \sum_{i=2}^{N} \left(\frac{\Delta T_{i,j} + \Delta T_{(i-1),j}}{2} \right) \Delta\psi \tag{2.21}$$

using the trapezoidal method, where i is the counter in the spanwise direction and the azimuth discretization is

$$\Delta\psi = \frac{2\pi}{M} \tag{2.22}$$

where M is the number of time stepping sections over the azimuth and j is the counter in the azimuth (time) direction.

The corresponding coefficient of thrust of the main rotor is

$$C_{TMR} = \frac{T_{MR}}{\rho\, A\, (\Omega R)^2} \tag{2.23}$$

The increment in induced power along the span is calculated by

$$dP_i = dL \sin\phi\ \Omega y \tag{2.24}$$

and the corresponding increment in profile power is calculated along the span by

$$dP_0 = dD \cos\phi\ \Omega y \tag{2.25}$$

Numerically, increments in induced and profile power can be expressed as,

$$\Delta P_i = \Delta L \sin\phi\ \Omega y \tag{2.26}$$

$$\Delta P_\circ = \Delta D \cos\phi\ \Omega y \tag{2.27}$$

Let P_s be the sum of the induced power and the profile power, i.e.,

$$dP_s = dP_i + dP_\circ \tag{2.28}$$

Numerically, it can be written as,

$$\Delta P_s = \Delta P_i + \Delta P_\circ \tag{2.29}$$

The total power for the main rotor is

$$P_{\mathrm{MR}} = \frac{N_b}{2\pi} \int_0^{2\pi} \int_0^R dP_s \, d\psi \tag{2.30}$$

Numerically, the power is obtained from a sum along the span and around the azimuth using

$$P_{\mathrm{MR}} = \frac{N_b}{4\pi} \sum_{j=2}^{M} \sum_{i=2}^{N} \left(\frac{\Delta P_{s_{i,j}} + \Delta P_{s_{(i-1),j}}}{2} \right) \Delta\psi \tag{2.31}$$

Then the power coefficient is calculated using

$$C_{P_{\mathrm{MR}}} = \frac{P_{MR}}{\rho A (\Omega R)^3} \tag{2.32}$$

Parasitic power is the power loss from the airframe, rotor hub, etc. is already a pre-integrated value and is given by

$$C_{P_P} = \frac{1}{2} \left(\frac{f}{A} \right) \mu^3 \tag{2.33}$$

where f is the equivalent drag area of the airframe. Therefore, the total power for the helicopter is the sum of main rotor power and parasitic power and is given by

$$C_P = C_{P_{\mathrm{MR}}} + C_{P_P} \tag{2.34}$$

The rotor drag can be also calculated by integrating the spanwise drag components over the azimuth, i.e.,

$$H_{\mathrm{MR}} = \frac{N_b}{2\pi} \int_0^{2\pi} \int_0^R dD \, sin(\psi) \, d\psi \tag{2.35}$$

The coefficient form of the rotor drag is,

$$C_H = \frac{H_{MR}}{\rho A(\Omega R)^2} \tag{2.36}$$

The rotor drag in coefficient form can hence be expressed as,

$$C_H = \frac{N_b}{2\pi\rho A(\Omega R)^2} \int_0^{2\pi} \int_0^R dC_D \; sin(\psi) \; d\psi \tag{2.37}$$

Numerically, the rotor drag coefficient is calculated using

$$C_H = \frac{N_b}{4\pi\rho A(\Omega R)^2} \sum_{j=2}^{M} \sum_{i=2}^{N} \left(\frac{\Delta C_{D_{i,j}} + \Delta C_{D_{(i-1),j}}}{2} \right) \Delta\psi \tag{2.38}$$

where ΔC_D can be obtained from Eqs. 2.8 and 2.48.

Rotor drag can then be calculated using,

$$H_{\mathrm{MR}} = \rho A(\Omega R)^2 C_H \tag{2.39}$$

2.1.3 Blade Flapping

Blade flapping about the hinge affects the value of U_P and hence the angles of attack over the rotor blade, i.e.,

$$U_P = \lambda(y, \psi) + \dot{\beta}(y - eR) \tag{2.40}$$

where the blade flapping velocity is given by $\dot{\beta} = d\beta(\psi)/dt$ and the hinge is located at a distance eR from the rotational axis. The governing equation for blade flapping is

$$\ddot{\beta} + \nu_\beta^2 \, \beta = \gamma \bar{M}_\beta \tag{2.41}$$

where γ is the Lock number, ν_β is flapping frequency and $\bar{M}_\beta$ is the aerodynamic moment about the flapping hinge as given by

$$\bar{M}_\beta = \frac{1}{\rho \; C_{l\alpha} \; c \; R^4 \; \Omega^2} \int_0^R L \; y \; dy \tag{2.42}$$

where ρ is the air density at flight altitude, L is lift force distribution across the blade, and $C_{l\alpha}$ is lift curve slope of the airfoil and is assumed to be 2π/rad.

The flapping frequency is obtained in terms of the non-dimensional hinge offset, e, where

$$\nu_\beta = \sqrt{1 + \frac{3\,e}{2(1-e)}} \tag{2.43}$$

and the Lock number is

$$\gamma = \frac{\rho\,\overline{C_{l\alpha}}\,c\,R^4}{I_b} \tag{2.44}$$

where I_b is the mass moment of inertia about the flapping hinge. For this thesis, the Lock number was assumed to be 8 obtained from [Ref. 3].

To solve the foregoing flapping equation, it was first split into a system of two first order equations, i.e.,

$$\dot{\beta_1} = \beta_2 \tag{2.45}$$

and

$$\dot{\beta_2} = -\gamma\,\bar{M}_\beta - \nu_\beta^2\,\beta_1 \tag{2.46}$$

These two latter equations were then solved in MATLAB using the ode45 solver. According to [Ref. 37], ode45 is used to solve differential equations and is quite robust and versatile. The solver does require initial conditions to start the computations, which are $\beta = 0$ and $\dot{\beta} = 0$. After the first iteration, the initial conditions are the previous calculated β and $\dot{\beta}$. The time step ran from the previous time step to the current time step.

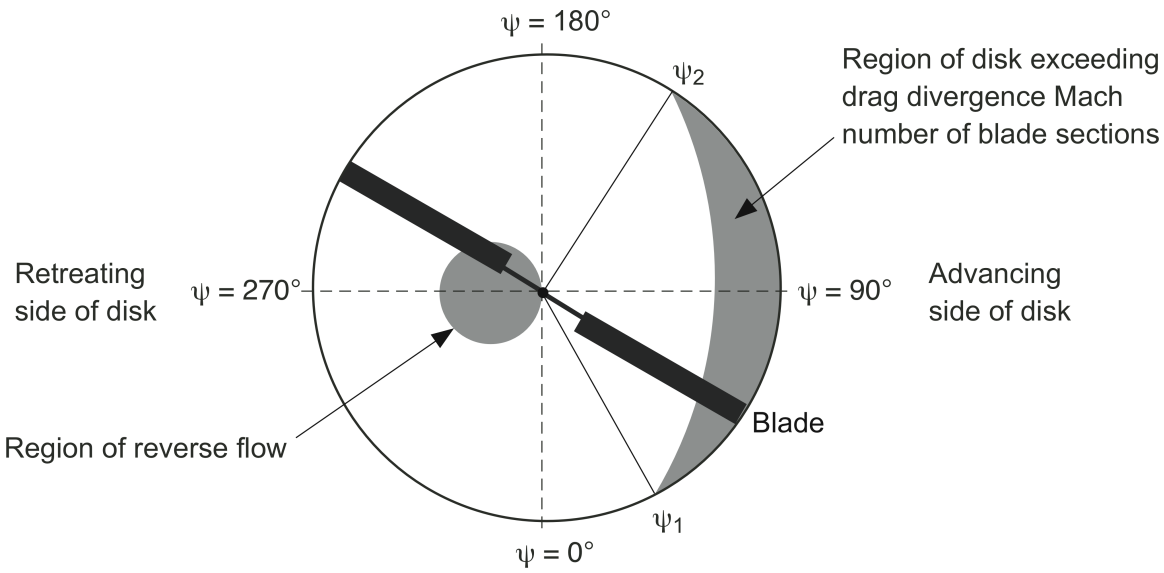

Figure 2.4: Compressibility and reverse flow regions on the rotor disk.

2.1.4 Airfoil Characteristics

As seen from Fig. 2.4, a rotor has its airfoil performing under varying conditions including high subsonic Mach numbers and reverse flow. Compressibility affects the lift curve slope and needs to be corrected using the Glauert correction factor, $\beta(\mathrm{M})$. Reverse flow region occurs on the retreating side of the rotor where the blade sections operate with their trailing edges into the wind. This relates to the blade sections operating at higher angles of attack to compensate for the difference in lift. Hence, the airfoil sections function closer to stall on the retreating side than the advancing side. Also, U_T and the sectional drag coefficient change in the reverse flow region.

Compressibility issues occur on the advancing side of the rotor where the tip of the blades approach and exceed drag divergence Mach number. The drag divergence Mach

number, M_{dd}, is the Mach number at which drag begins to rapidly increase. Drag divergence leads to the drag increasing quickly at the tip. The increment is modeled by,

$$\Delta C_d = 12.5\ (M - M_{dd})^3 \tag{2.47}$$

when $M\ \geq M_{dd}$. Drag divergence Mach number, M_{dd}, is set to 0.8 for SC1095 airfoil.

The forgoing were taken into account by the following steps:

1. The reverse flow region was taken into consideration when $U_T < 0$

$$C_d = 3\ C_d \tag{2.48}$$

2. Compressibility effects on the lift curve slope, i.e., for the Mach number

$$M = \frac{U_T}{a} \tag{2.49}$$

where $a = \sqrt{\gamma\, R\, T}$. The effect on local lift curve slope is

$$C_{l_\alpha} = \frac{2\pi}{\sqrt{1 - {M_\infty}^2}} \tag{2.50}$$

where 2π is the lift curve slope in incompressible flow.

3. If $C_l > C_{l_{\max}}$, where $C_{l_{\max}}$ is the maximum sectional lift coefficient of 1.5. The calculations are stopped because exceeding maximum sectional lift coefficient indicates the onset of blade stall.

2.2 Rotor Trim

A trim procedure was needed to trim the rotor before the coefficients can be calculated. Figure 2.5 shows the forces acting on a helicopter in forward flight.

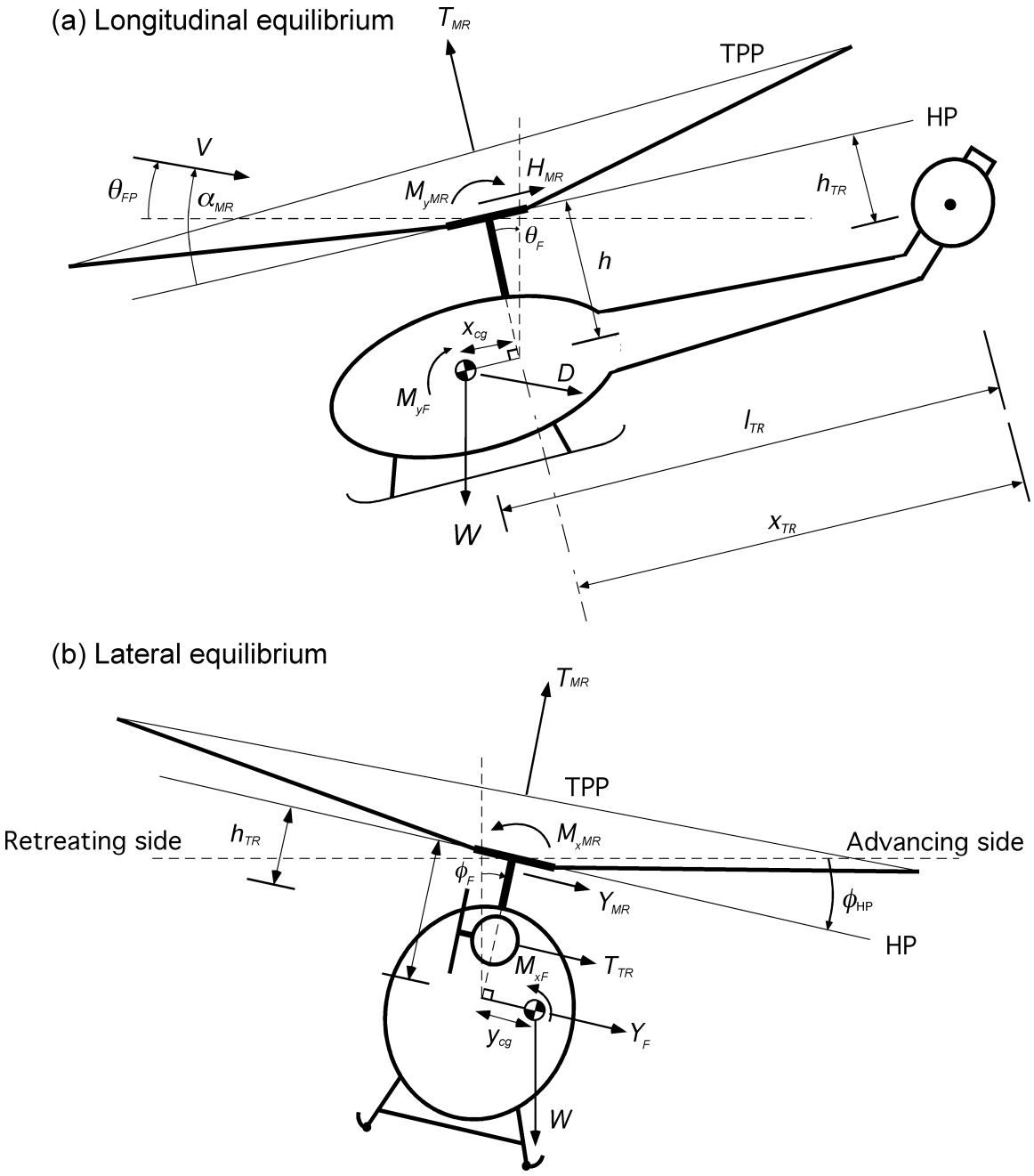

Figure 2.5: Forces on a helicopter in forward flight.

After the blade flapping was calculated, the Fast Fourier Transform (FFT) [Ref. **?**] was taken of the 10^{th} revolution of the rotor. The 10^{th} revolution was used to make sure

that the rotor had settled into its steady state flapping response. This FFT provides the first two amplitudes corresponding to β_{1c} and β_{1s}, and the higher harmonics are small and are ignored.

The trim matrix is

$$\begin{bmatrix} C_T \\ \beta_{1c} \\ \beta_{1s} \end{bmatrix} = \begin{bmatrix} \frac{dC_T}{d\theta_0} & \frac{dC_T}{d\theta_{1c}} & \frac{dC_T}{d\theta_{1s}} \\ \frac{d\beta_{1c}}{d\theta_0} & \frac{d\beta_{1c}}{d\theta_{1s}} & \frac{d\beta_{1c}}{d\theta_{1c}} \\ \frac{d\beta_{1s}}{d\theta_0} & \frac{d\beta_{1s}}{d\theta_{1c}} & \frac{d\beta_{1s}}{d\theta_{1s}} \end{bmatrix} \begin{bmatrix} \theta_0 \\ \theta_{1s} \\ \theta_{1c} \end{bmatrix} = J \begin{bmatrix} \theta_0 \\ \theta_{1s} \\ \theta_{1c} \end{bmatrix}$$

where J is the Jacobian and denotes the relationship between the control inputs and the rotor trim variables. The right hand side of the above equation has to converge to 0 ± 0.1 for the rotor to be trimmed. Tolerances needed to be set for the code to converge, which were:

- Amplitude corresponding to $\beta_{1c} <= 0.1$

- Amplitude corresponding to $\beta_{1s} <= 0.2$

- Amplitude corresponding to $\beta_0 <= 0.05$

When the three flight controls (θ_0, θ_{1c} and θ_{1s}) were obtained, they were used in the main rotor code. While this procedure trimmed the rotor sufficiently well at low and moderate airspeeds, the rotor could not be trimmed at speeds above 160 knots and hence, all calculations were conducted until 160 knots was reached.

From Fig. 2.6, α_{TPP} is calculated using propulsive trim, i.e., when the propulsive force component of the rotor thrust is equal to drag. The drag of the airframe is calculated using

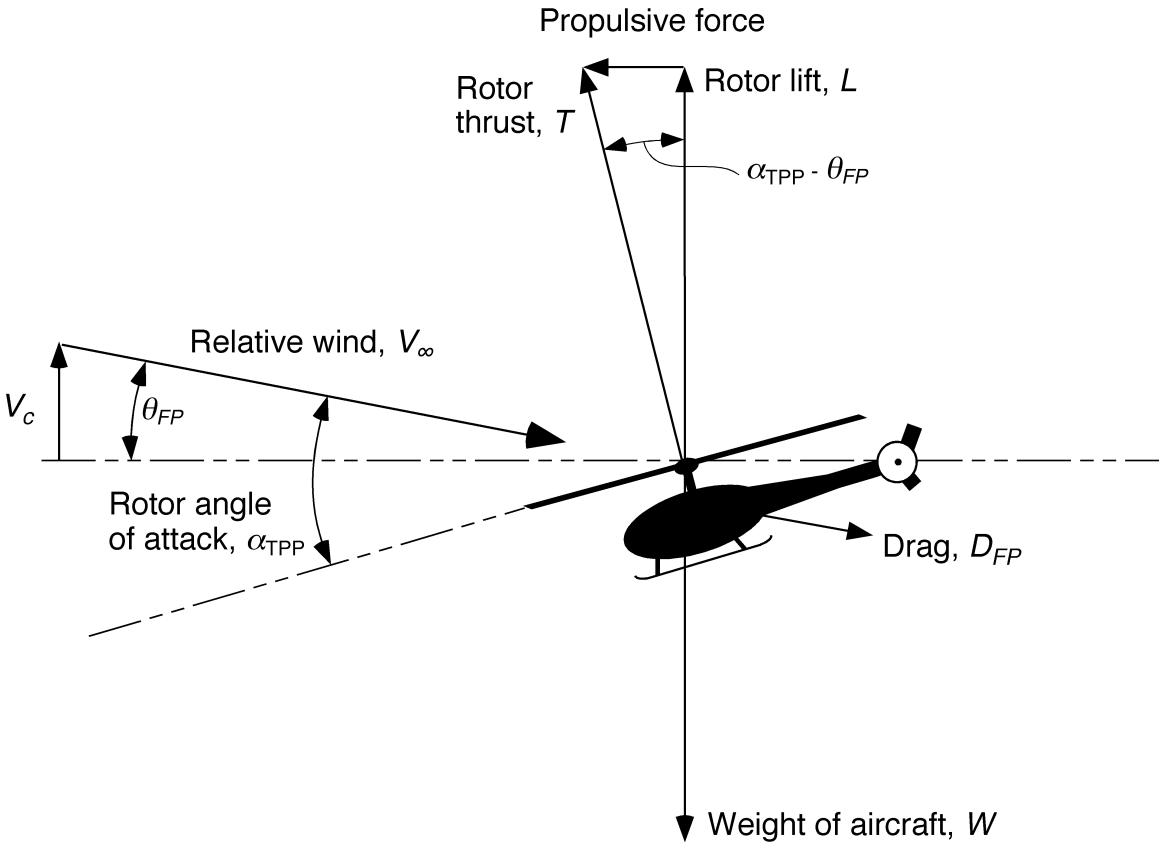

Figure 2.6: Forces acting on a helicopter in forward flight.

equivalent flat plate area, f, of a UH-60 helicopter which is 23 ft^2. The drag on the airframe is given by

$$D_f = \frac{1}{2}\,\rho\, V_\infty^2\, f \tag{2.51}$$

so the angle of attack of the tip path plane for propulsive trim is then calculated using

$$\sin \alpha_{TPP} = \frac{D_f}{T_{MR}} \tag{2.52}$$

From Fig. 2.6, it can be seen that rotor thrust has two components, one to overcome weight of the aircraft and the other to overcome drag of the airframe. Hence, α_{TPP} had to be set such as to produce the required total rotor thrust to overcome both weight and drag.

To achieve this, an initial α_{TPP} of 0.1° was set and the thrust required was calculated. If the rotor cannot be trimmed, then α_{TPP} is increased until the required thrust is produced. The control angles θ_0, θ_{1c} and θ_{1s} were adjusted accordingly as part of the overall trim procedure to obtain the required C_{T} value and rotor orientation.

Endurance is the maximum amount of time an aircraft can stay in cruise and is typically calculated using the Breguet equation obtained from [Ref. 38]. For a rotorcraft at constant velocity and altitude,

$$\frac{dW_\circ}{dt} = (SFC)\, P \tag{2.53}$$

where SFC is the specific fuel consumption and is assumed to be $0.45 \frac{\text{lb}}{\text{hp hr}}$ for the UH-60, P is the power required to attain level cruise flight at given altitude and velocity and the ratio $\frac{\text{dW}_\circ}{\text{dt}}$ is the fuel consumption in lb/hp/hr.

Integrating from time t_1 to t_2

$$\int_{t_2}^{t_1} dt = \int_{W_1}^{W_\circ} \frac{dW_\circ}{(SFC)\, P} \tag{2.54}$$

Assuming constant specific fuel consumption (SFC),

$$t_2 - t_1 = \frac{1}{(SFC)\, P} \left(W_\circ - W_1\right) \tag{2.55}$$

The gross takeoff weight ($W_\circ$) can be written in terms of fuel weight (W_f) and weight of aircraft without any fuel (W_1) as,

$$W_\circ = W_1 + W_f \tag{2.56}$$

The endurance ($t_1 - t_2$), can thereby be written as

$$E = \frac{W_f}{(SFC)\, P} \tag{2.57}$$

The UH-60 carries approximately 360 gallons of fuel [Ref. 39]. One gallon of fuel equates to about 6.7 lbs. Hence, the helicopter carries 2412 lbs of fuel.

3. Results and Discussion

3.1 Validation

Representative parameters of the UH-60A Blackhawk were used to validate the method, the key values being shown in Table 3.1.

Table 3.1: Parameters used for the validation.

Parameters	**Value**
Weight	16,000 lb
Chord	1.73 ft
Main Rotor Radius	27 ft
Number of Blades (N_b)	4
Blade Twist (θ_{TW})	-18°
V_{tip}	725 ft/sec
C_{do}	0.008

Using outcomes from the model described in Chapter 2, the spanwise variations of inflow, coefficient of thrust and lift for different linear twist rates are shown in Figs. 3.1, 3.2 and 3.3.

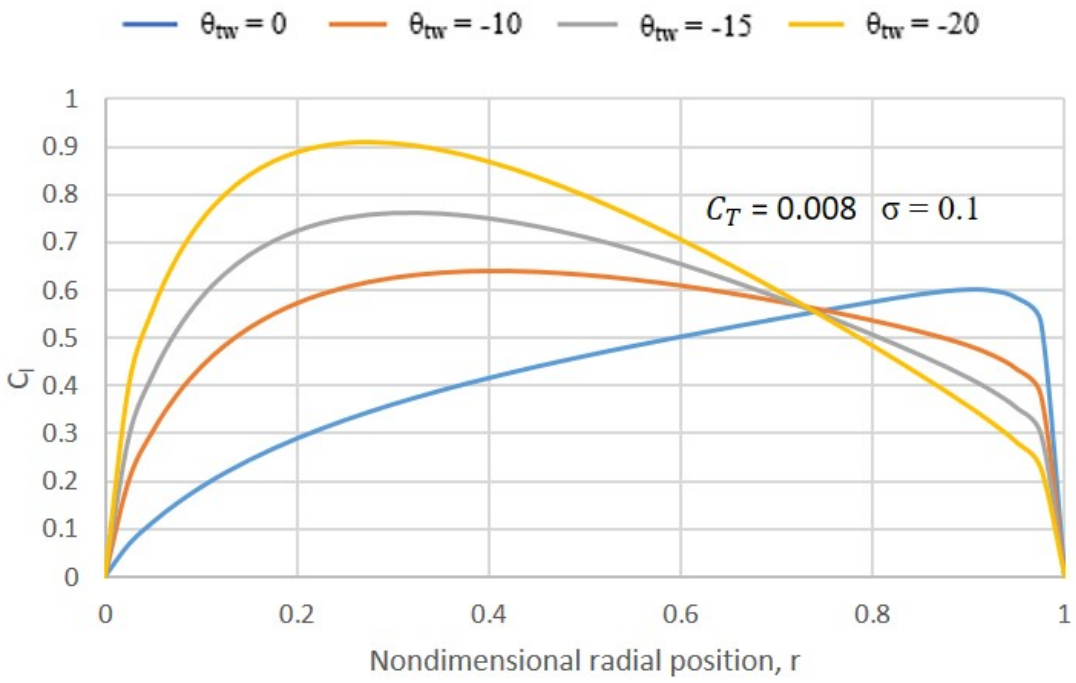

Figure 3.1: Lift distribution for different linear twists.

These results are in excellent agreement to the ones found in [Ref. **?**]. Notice from Fig. 3.1 that increasing blade twist redistributes the lift over the blade makes the distribution increasingly more linear, i.e., closer to the ideal case. From the results Fig. 3.2, it can also be noted that with higher blade twist, the thrust distribution over the blade decreases towards the tip and is considerably more near the mid-span. As seen from Fig. 3.3, increasing twist affects the inflow, and with higher twist there is lower inflow at the tip and more near the mid-span of the blade. Shown in Fig. 3.4 is the amount of collective pitch needed for various twist rates at a σ of 0.1.

From Fig. 3.5, it can be seen that blade flapping response (β) converges to the same value regardless of initial condition, as it should. Figure 3.6 shows the blade flapping

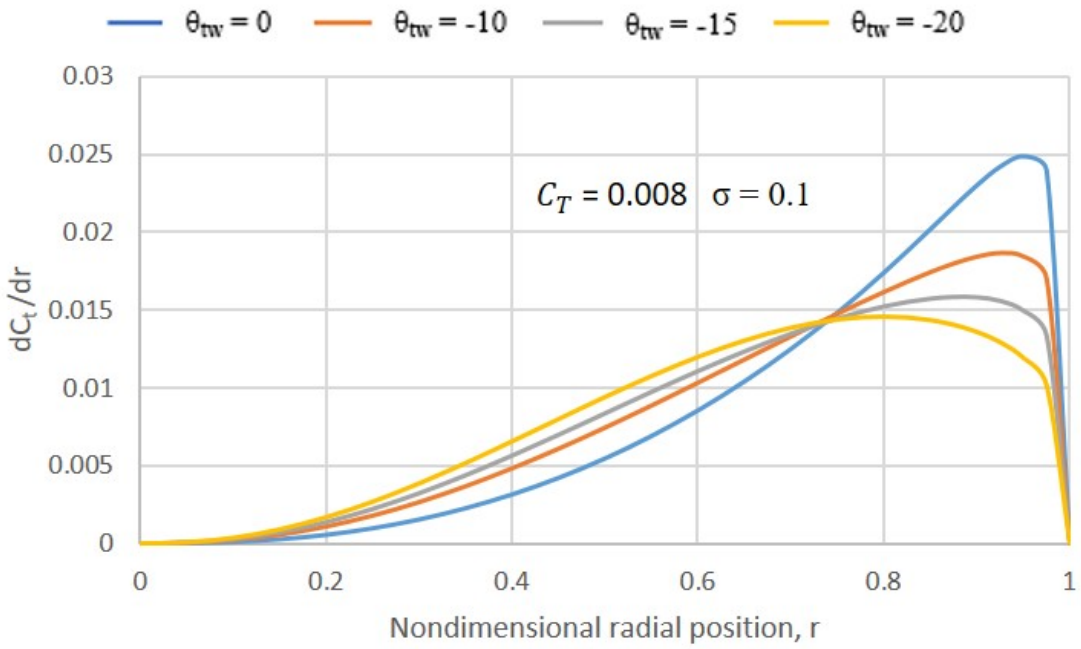

Figure 3.2: Thrust distribution for different linear twists.

response at 60 knots. It can be noted that the rotor blade flaps up at around 180° and flaps down at 360° denoting the rotor, without being trimmed using θ_{1c} and θ_{1s}, is tilting backward and to the left.

After the rotor is trimmed using the collective, lateral cyclic, and longitudinal cyclic, i.e., θ_0, θ_{1c} and θ_{1s}, the forward flight blade flapping response obtained is shown in Fig. 3.7. It can be observed that the rotor flaps up at around 360° and flaps down at approximately 180°, which shows that the rotor disk is now tilted forward at α_{TPP} of 4.5° to meet the propulsion requirement.

Figure 3.8 shows the comparison between the flapping responses obtained from flight test [Ref. **?**] to the responses attained from the current method. The power as well as

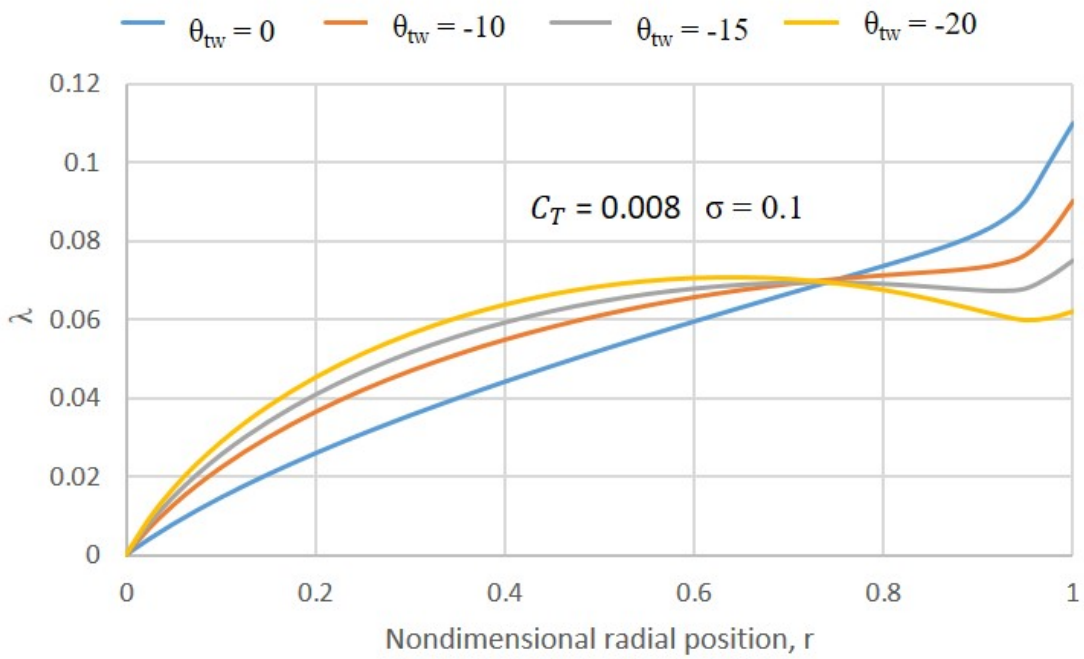

Figure 3.3: Inflow distribution for different linear twists.

the lift-to-drag ratio curves were to be compared but flight test data is not available for all airspeeds. The data available are taken from [Ref. **?**] and are plotted against the values generated by the present method.

From Figs. 3.9 and 3.10, it can be seen that the power is under predicted, especially at higher airspeeds. Similarly, lift to drag ratio is slightly under predicted as well.

Chopra [Ref. 32] conducted research on a rotor with variable radius and variable rpm, which was done using the University of Maryland Advanced Rotor Code (UMARC).

From the results in Figs. 3.11 and 3.12, it can be seen that the difference between the present method and UMARC is of the order of 10–40 hp. A maximum difference of 40 hp occurs at 120 knots, as shown in Fig. 3.12, while a minimum difference of 5 hp occurs at

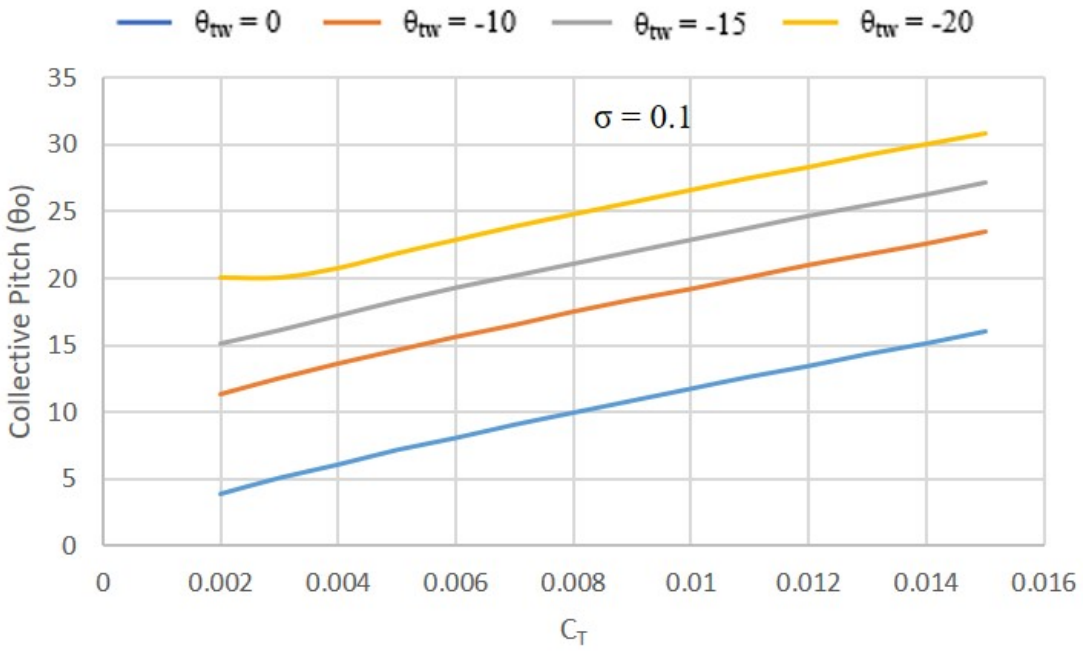

Figure 3.4: Collective pitch variations with thrust at hover.

140 knots, as shown in Fig. 3.11. The present method under predicts the power as compared to UMARC.

The flight endurance of the UH-60 is roughly 2.1 hours at 150 knots [Ref. 40]. From Eq. 2.57, the endurance obtained was 2.14 hours at the same airspeed, this difference translates to approximately 3 minutes.

3.2 Blade Morphing: Varying Single Parameters

Four blade and rotor morphing strategies were considered: varying blade twist, varying rotor rpm, varying rotor radius and varying blade chord. The objectives were to assess the effects on rotor power and drag as a function of airspeed and also aircraft weight.

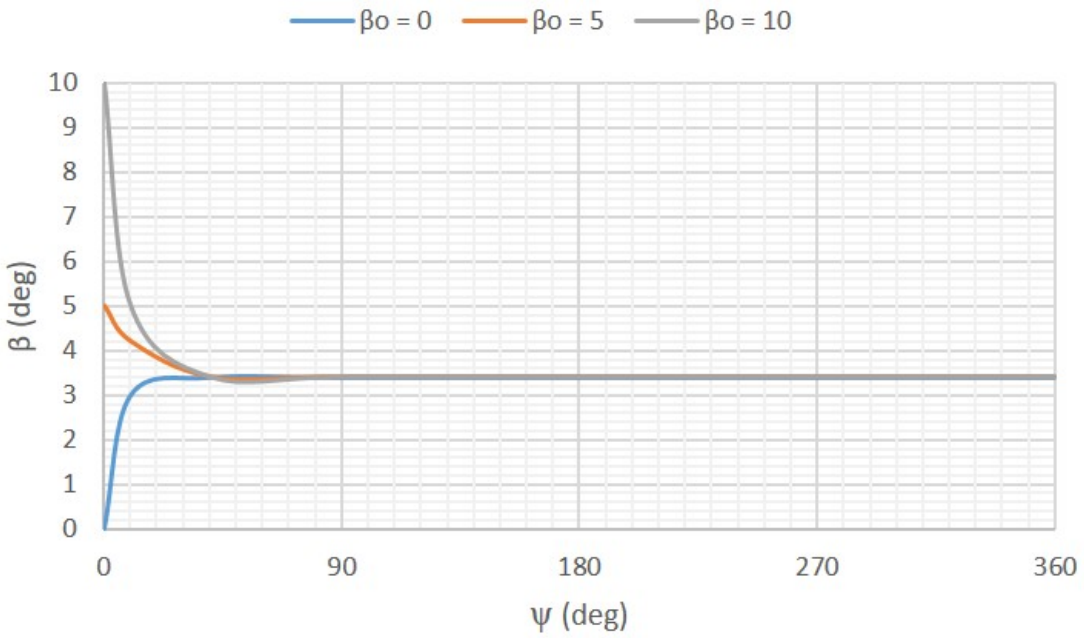

Figure 3.5: Flapping response for different initial values of β_0.

To begin with, the impact of varying individual elements (e.g., only blade twist or only rotor speed etc.) were considered. Then, the rotor was morphed as a function of airspeed. Finally, combinations of blade and rotor morphing were analyzed to assess the possible best outcomes in terms of overall rotor performance.

3.2.1 Blade Twist Variations

An analysis of linear blade twist rate of $\theta_{TW} = 0°, -5°, -10°$ and $-15°$ per radius were conducted. The inboard sections of the blade stalled with $-20°$ linear twist because a higher θ_0 was required for thrust trim, and hence the inboard sections operated at higher angles of attack that reached the stall limit.

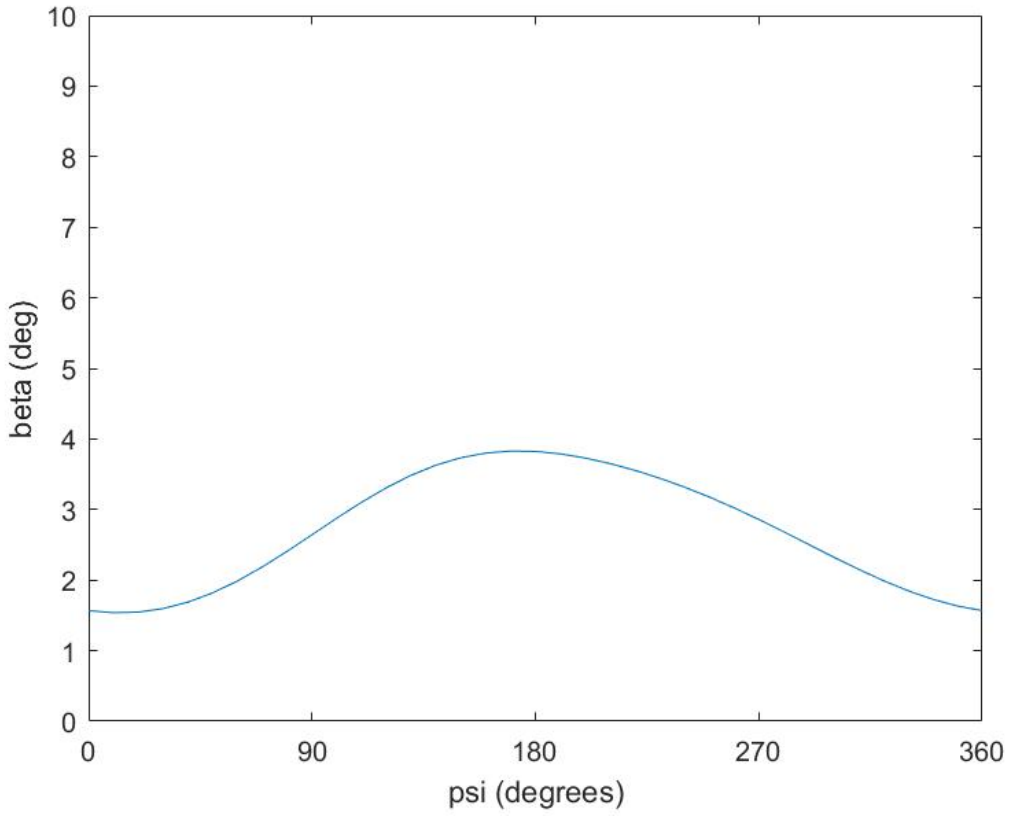

Figure 3.6: Flapping response at airspeed of 60 knots before trimming.

The power curves, as shown in Fig. 3.13, that were calculated with the various blade twist rates show that higher twist was required to minimize power during hover but much less or even no twist is beneficial during forward flight. In hover, there is a axisymmetrical distribution of lift over the entire rotor disk, and hence more twist would be beneficial to improve the uniformity of the inflow. The risk is that with too much blade twist the highest lift coefficients move inboard increasing the propensity to stall there, as seen from Fig. 3.1.

Similarly, in forward flight, higher amounts of twist lead to higher values of collective pitch θ_0 to trim, and hence the angles of attack at the inboard sections are higher and

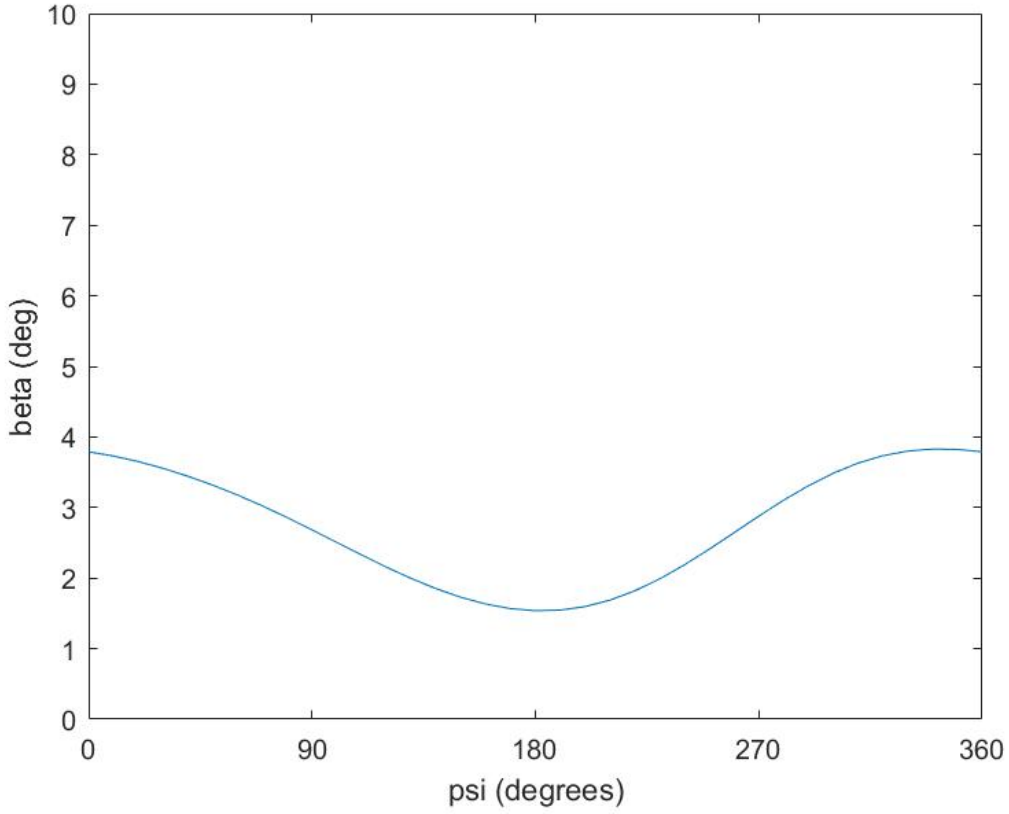

Figure 3.7: Flapping response at 60 knots after being trimmed to meet propulsive requirement with $\alpha_{TPP} = 4.5°$.

thereby more likely to stall. Notice that the power requirements decrease by 10% at 160 knots without any blade twist compared to the baseline case, which is equivalent to a 150 hp decrease in power for the UH-60. Putting this result into perspective, means that if the UH-60 carries approximately 2,412 lb of fuel, for a 2 hour flight leads to an extended endurance of approximately 8 minutes.

An analysis of the results from Fig. 3.14 for rotor drag reveals that rotor drag is relatively the same at low to moderate airspeeds but decreases by approximately 30% at higher

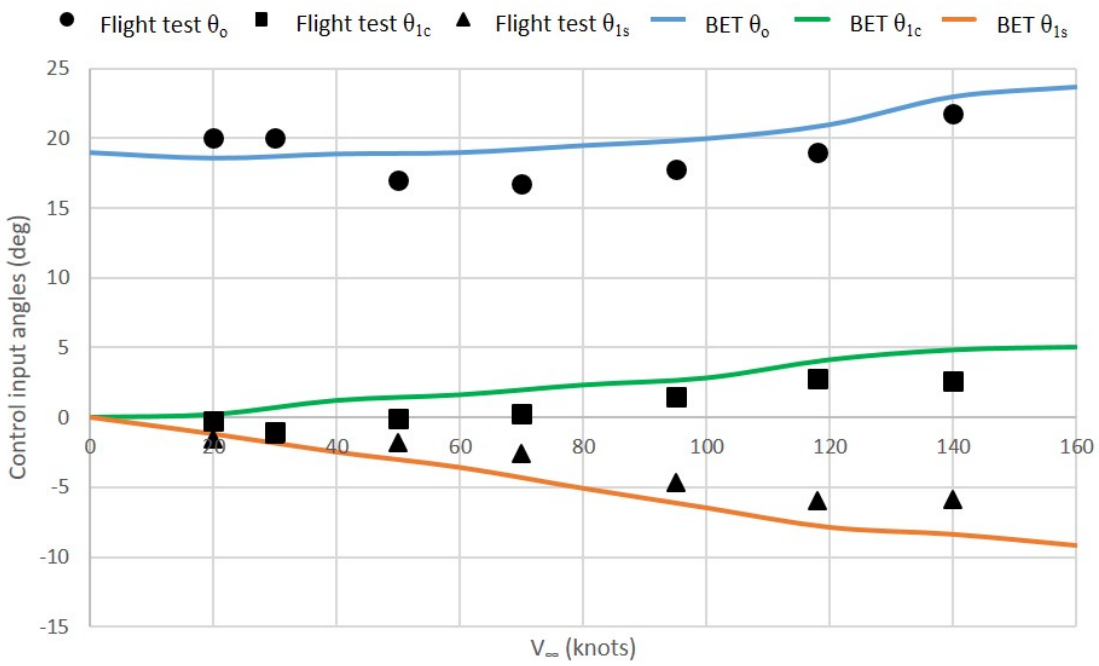

Figure 3.8: Comparison of control input angles between flight test and current method.

airspeeds; this 30% change is around 260 lb of drag in this case. The use of higher blade twists seem to lead to higher rotor drag at higher airspeeds.

The comparisons made of the lift-to-drag ratios from the results in Fig. 3.15 reveals that the ratio is relatively similar for all blade twists at low to moderate airspeeds. The maximum changes occur at higher airspeeds and gives a lift-to-drag ratio differences of about 0.5 from the baseline. Also, at 140 knots, the lift-to-drag ratio is nearly the same for blade twists of $\theta_{TW} = 0^\circ$ and -5°.

From the results in Fig. 3.16, it can be observed that higher blade twist require more rotor thrust for the same forward speed, the total thrust being comprised of the thrust needed to overcome weight and the extra thrust needed to overcome rotor and airframe drag.

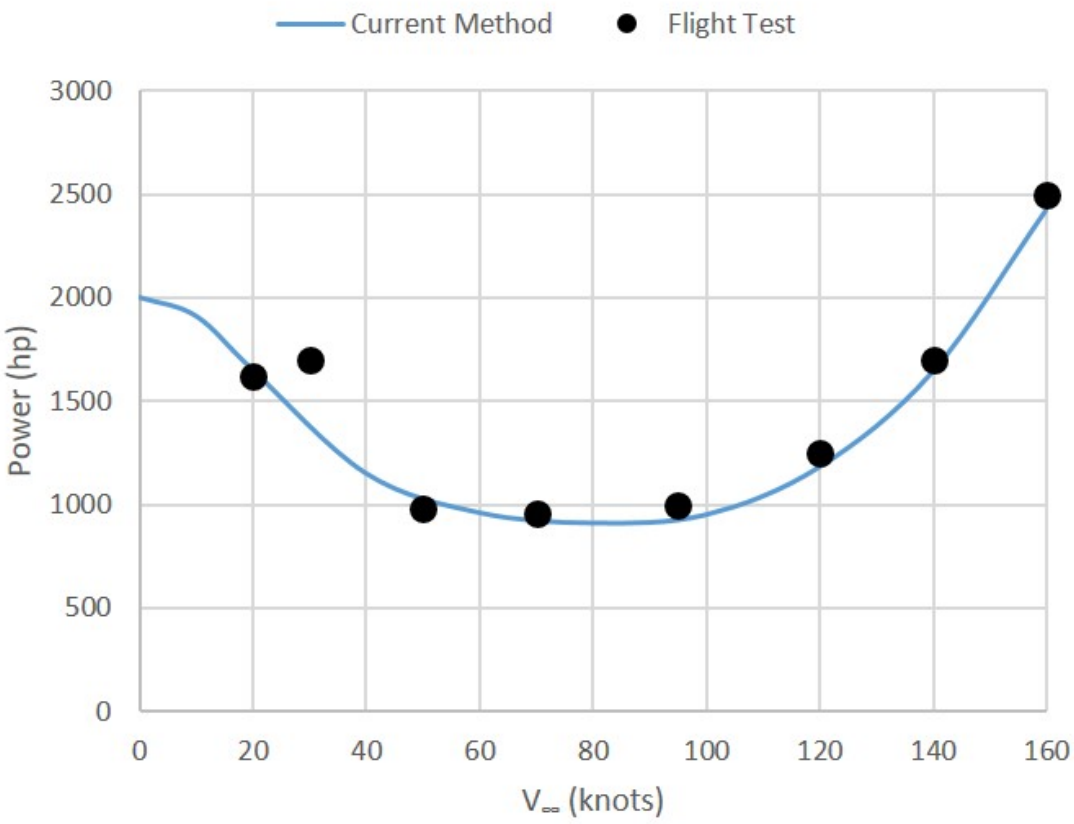

Figure 3.9: Power comparison between current method and test flight for the UH-60 (Weight = 16,000 lb and altitude = 5,200 ft).

3.2.2 Rotor Radius Variations

The effects of rotor radius reductions of 5% and 10% were analyzed. Because lower values of blade radius led to premature blade stall issues (not enough blade area to carry the the thrust without stall), further reductions in radius were not made. Decreasing radius leads to a smaller rotor disk areas and blade areas and hence the blade sections must now

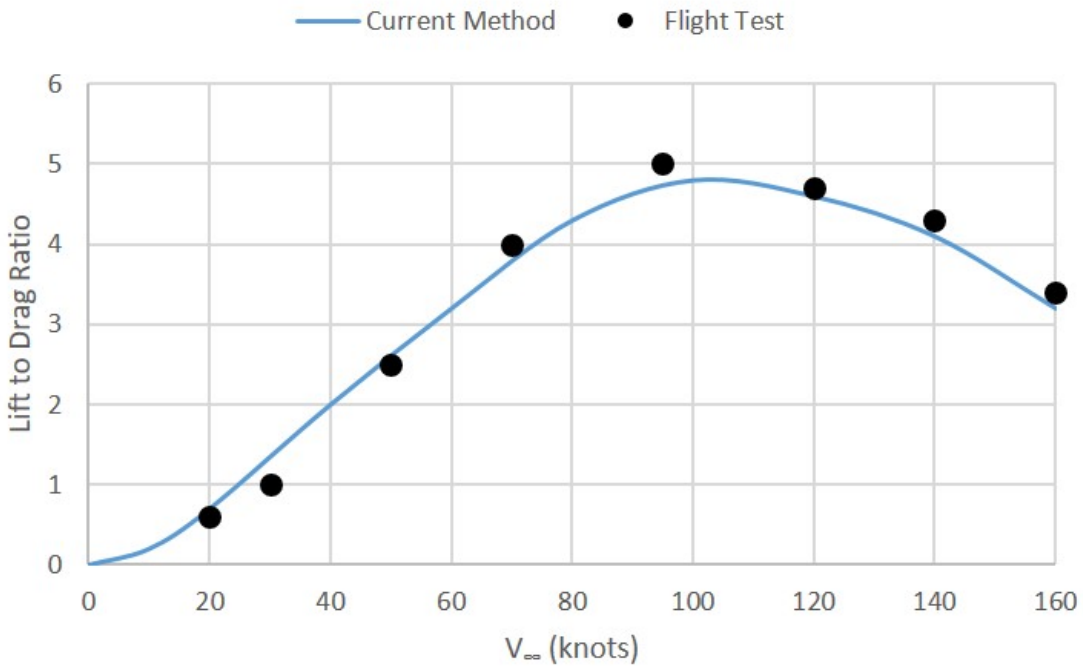

Figure 3.10: Lift-to-drag ratio comparison between current method and test flight for the UH-60.

operate at higher angles of attack to generate the same total thrust. This all leads very quickly to a higher possibility of stall as the blade radius is shortened.

Notice from Fig. 3.17 that the power requirements in hover increases with a radius reduction, which is a direct consequence of rotor operation at a higher disk loading. For fixed tip speeds, the power requirements decrease with increasing values of θ_{TW}. However, in forward flight a power savings of approximately 180 hp can be obtained at 160 knots for a 10% reduction in rotor radius. At moderate and higher airspeeds, a reduction of radius leads to a decrease in total power requirements. At lower airspeeds, the power requirements are generally higher for reductions in rotor radius, with the 10% radius reduction being the

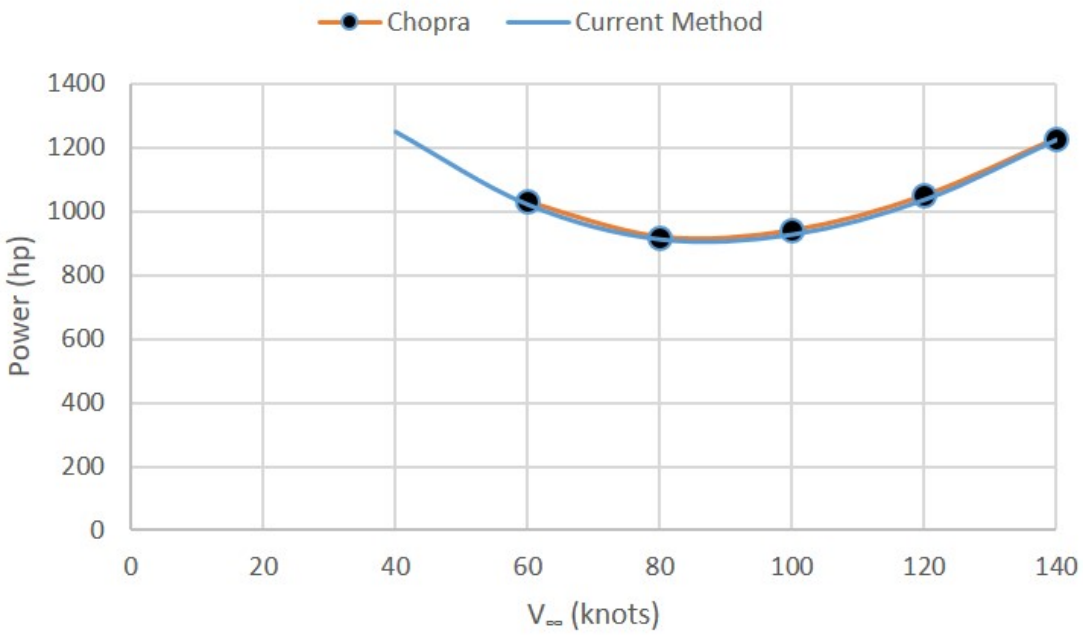

Figure 3.11: Power comparison for variable radius between the present method and [Ref. 32] (W = 18,000 lb).

most that could be used without promoting blade stall. Also note that only reductions in power occur only after an airspeed of 120 knots is reached.

As shown in Fig. 3.18, the corresponding lift-to-drag ratio remains similar at low and moderate airspeeds and modestly increases at higher airspeeds with a maximum difference of 0.4 at 100 knots for a 10% reduction in rotor radius. The reason for these outcomes comes from a reduction of rotor drag, as can be inferred from Fig. 3.19. Nevertheless, the difference between the two lift-to-drag ratio curves is small, with any difference being apparent only at higher airspeeds.

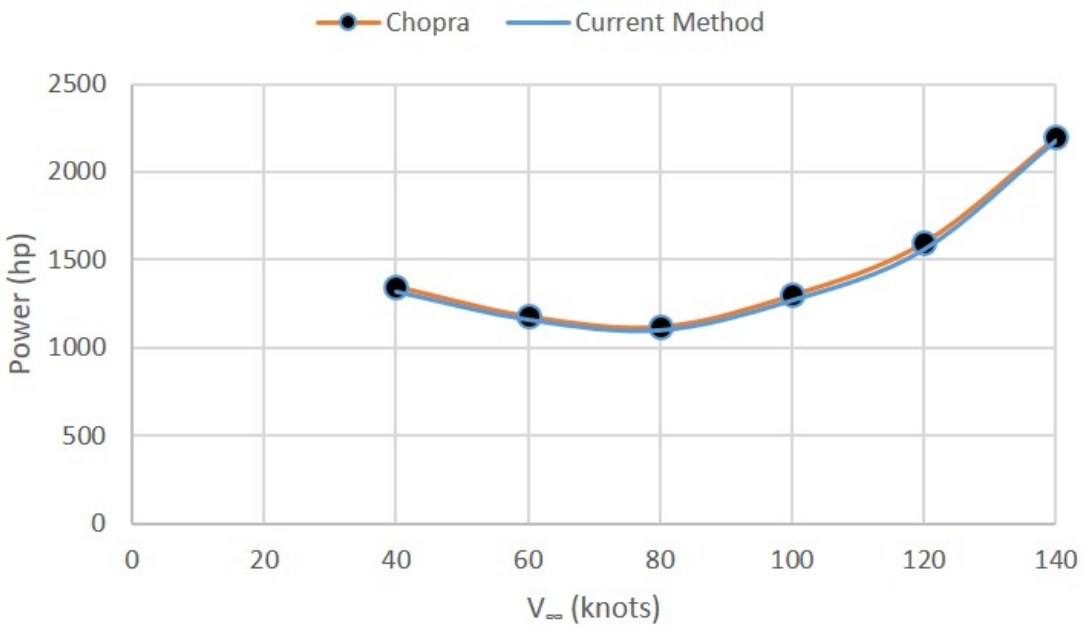

Figure 3.12: Power comparison for variable RPM between the present method and [Ref. 32] (W = 18,400 lb).

Because a propulsive trim requirement was imposed, i.e., the sum of rotor drag and airframe drag is equal to forward propulsive thrust, the total thrust required shows a small decrease with a reduction in blade radius because of the reduction in rotor drag. This can be seen in Fig. 3.20. From Fig. 3.19, it can be seen that a maximum drag reduction of approximately 150 lb can be achieved at 160 knots by decreasing the rotor radius by 10%.

3.2.3 Rotor Speed (rpm) Variations

Rotor speed was reduced by 5% and 10% for analysis purposes. With reductions up to 15%, stall issues were found on the retreating side of the rotor disk at 60 knots and above.

Recall that reducing rotor speed leads to the blade sections operating at higher angles of attack to produce a given lift, and hence they will generally all operate closer to the onset of stall than they would at higher rotor rpm.

From Fig. 3.21, it can be observed that the power required in hover and forward flight is considerably lower with reductions of rotor rpm. Although this does mean that the blades are operating closer to their maximum lift capabilities, there are still some power reductions to be obtained. A rotor with 5% rotor speed reduction requires slightly less power than for the baseline case, with a maximum power reduction of 170 hp obtained by reducing the speed by 10% at 160 knots. Recall that all of these observations are based on trimmed flight conditions.

The corresponding lift-to-drag ratio increases, as noted from Fig. 3.22, with a decrease in rotor rpm. A maximum difference of 0.6 is obtained at 100 knots with a 90% speed reduction. However, overall the differences between the two speed reduction cases are fairly small. As noted from the results in Fig. 3.23 and 3.24, the rotor drag was found to be close to the baseline case for both speed reductions, thereby having almost no effect on the total rotor thrust requirements.

3.2.4 Blade Chord Variations

An analysis of the effects of blade chord variations were conducted for chord changes of 5% and 10%. It was found that decreasing chord generally increased the operating angles of attack of the blade sections, and hence led to the onset of stall. As shown in Fig. 3.25, the power requirements were found to be modestly higher than the baseline case for 5%

and 10% increases in blade chord, which is a consequence of an increase in rotor drag from more blade surface area. As seen in Fig. 3.26, the drag is similar to the baseline case for both cases at low and moderate airspeeds while being modestly higher at higher airspeeds.

The corresponding lift-to-drag ratio is shown in Fig. 3.27, which decreases slightly as the ratio is inversely proportional to drag. Larger increases in chord length leads to lower rotor lift-to-drag ratios, as would be expected as the increased blade area increases rotor drag. The total rotor thrust shown in Fig. 3.28 increases with increasing chord length to reach propulsive trim requirement, the rotor drag being part of the total rotor thrust requirements.

3.3 Morphing Variations with Airspeed

In this section, several of the forgoing effects are morphed as a function of airspeed. For example, more blade twist is used in hover while lower amounts of twist were used at moderate and higher airspeeds. Hence, blade twist was morphed using a linear schedule such that it was -18° in hover and has reduced to 0° at 160 knots.

3.3.1 Individual Effects

Blade twist, rotor rpm, rotor radius and blade chord were morphed individually. As previously mentioned, blade twist was linearly changed such that it was -18° at hover to 0° at 160 knots. Rotor speed was changed according to the schedule that it was 100% at hover to 90% at 160 knots. Rotor radius was changed such that it was 100% at hover to

90% at 160 knots. Because there were no substantial benefits to be obtained by morphing the blade chord (i.e., too much chord increases rotor drag and too little chord increases the propensity to blade stall), it was not considered further in this study.

From an examination of Fig. 3.29 it can be seen that, at lower speeds, linear blade twist provides the most benefits with the maximum power reduction of 50 hp at 20 knots. At moderate speeds, changing speed results in a maximum power reduction of approximately 130 hp at 100 knots. At airspeeds between 100 and 150 knots, varying speed gives the most benefit compared to reductions in blade radius or blade twist. That being said, the appropriate use of blade twist does provide a 180 hp power reduction at 160 knots, which would account for approximately a 7% reduction in power.

At all airspeeds, as seen from Fig. 3.30, varying rotor speed provides the most gains in lift-to-drag ratio with a maximum gain of 0.6 at 100 knots. Morphing the rotor radius had lower gains to be obtained than by changing rpm, but higher benefit than morphing just the blade twist.

Changing rotor speed had almost no effect on rotor drag, while blade twist variations leads to the most drag reduction of approximately 300 lb at 160 knots, as can be seen from Fig. 3.31. Morphing the rotor radius leads to lower drag than the baseline, but more so than morphing blade twist alone. Inspecting Fig. 3.32, it can be seen that varying rotor radius requires more net rotor thrust than varying twist, but less than the baseline case as well as the varying speed case. Linearly morphing twist requires least amount of propulsive thrust because of the associated reduction in rotor drag.

3.3.2 Morphing Two Effects Together

Two morphing effects were varied simultaneously. For example, while twist was varied from -18° in hover to 0° at 160 knots, speed was simultaneously varied from 100% at hover to 90% at 160 knots. As shown in Fig. 3.33, varying twist and speed together was found to provide maximum power reductions at lower airspeeds of 20–50 knots, with the maximum reduction being 50 hp. For airspeeds between 60–100 knots, changing speed and radius together provides the most gains with a maximum reduction of 150 hp at 80 knots. At higher airspeeds of 110–150 knots, changing both blade twist and rotor radius together helped to obtain a maximum reduction of 280 hp at 140 knots. At 160 knots, reducing both speed and rotor radius helped to attain a 300 hp power reduction. Over a 2 hour flight time, this will extend the flight time by roughly 15 minutes.

From the results in Fig. 3.34, it can be seen that lift-to-drag ratio increases for all cases over the baseline rotor. Varying speed and radius provides the highest gains in lift-to-drag ratio at all airspeeds, with a maximum gain of 0.7 at 80 knots. The baseline rotor gives the lowest lift-to-drag ratio while varying twist and radius provides gains at all airspeeds. As shown in Fig. 3.35, rotor drag significantly decreases on varying twist and radius with a maximum drag reduction of 370 lb at 160 knots. Varying blade twist and radius together provides the second-best gains, while using speed and twist provides the least benefit. All cases provide more benefit than the baseline rotor. Recall that because this is a propulsive trim where forward propulsive thrust component is equal to the rotor drag, it can be

from Fig. 3.35 that morphing twist and radius linearly provides the least rotor drag at all airspeeds.

3.3.3 Morphing Three Effects Together

Three morphing effects were also varied simultaneously. For example, while twist was varied from -18° at hover to 0° at 160 knots, both rotor speed and radius was varied from 100% at hover to 90% at 160 knots. The power reductions were obtained at all airspeeds other than hover, as can be seen from Fig. 3.37. A maximum power reduction of 420 hp was attained at 160 knots, which results in fuel savings of 190 lb/hr and, hence, a total fuel saving of 380 lb over a 2 hour flight, and perhaps an extra flight time of approximately 20 minutes as calculated using Eq. 2.57. While this could be significant, unfortunately the blade sections function on the threshold of stall because of a reduction of both radius and rpm, so it is probably not a practical flight condition other than in perfectly smooth air.

The lift-to-drag ratio, as shown in Fig. 3.38, was better at every airspeed as compared to the baseline rotor with a maximum gain of 0.8 at 120 knots. This outcome is mainly because rotor drag, as seen from the results in Fig. 3.39, was significantly lower for the morphed rotor system than the baseline rotor with a maximum reduction of 300 lb occurring at 160 knots.

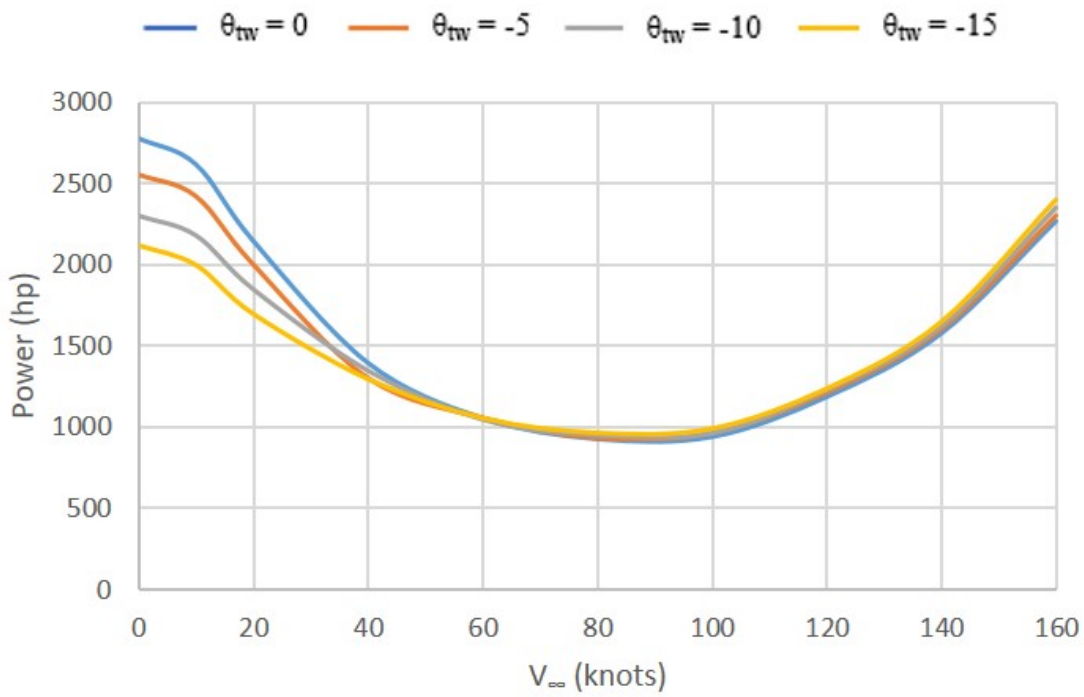

(a) Twist effect on Power

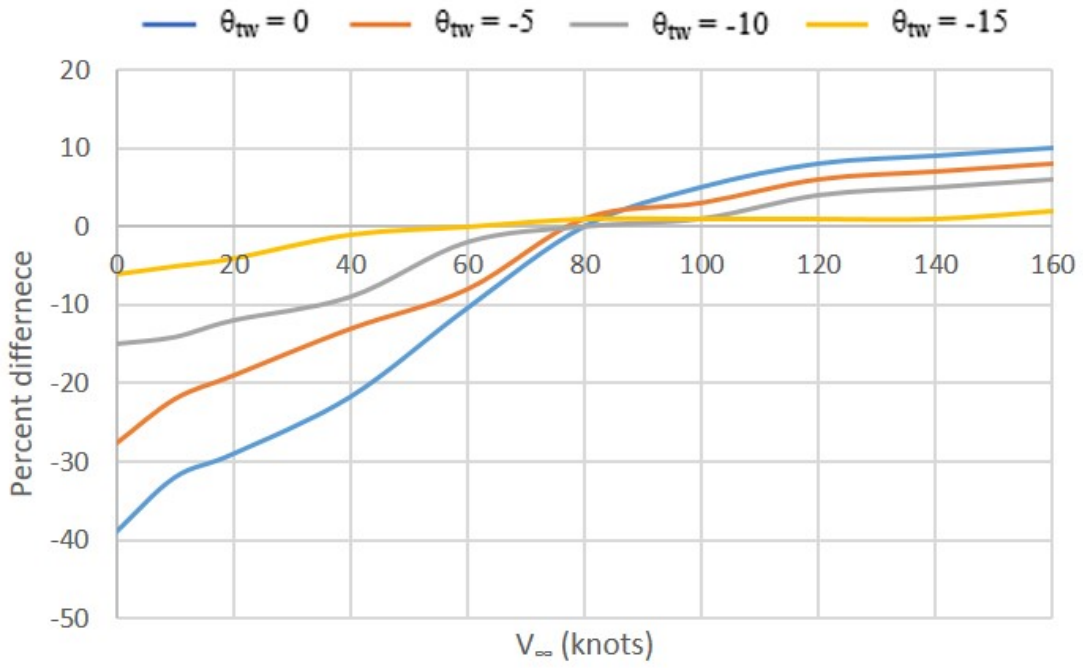

(b) Percent variance from the baseline case

Figure 3.13: Blade twist effect on power and variation from the baseline case.

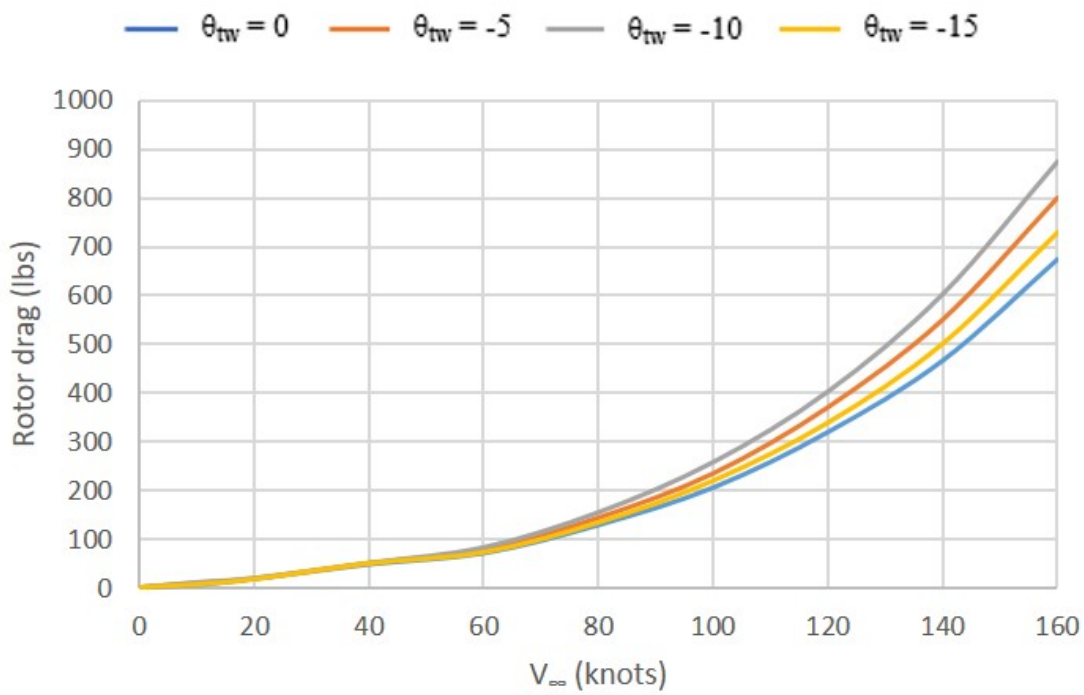

(a) Twist effect on Rotor Drag

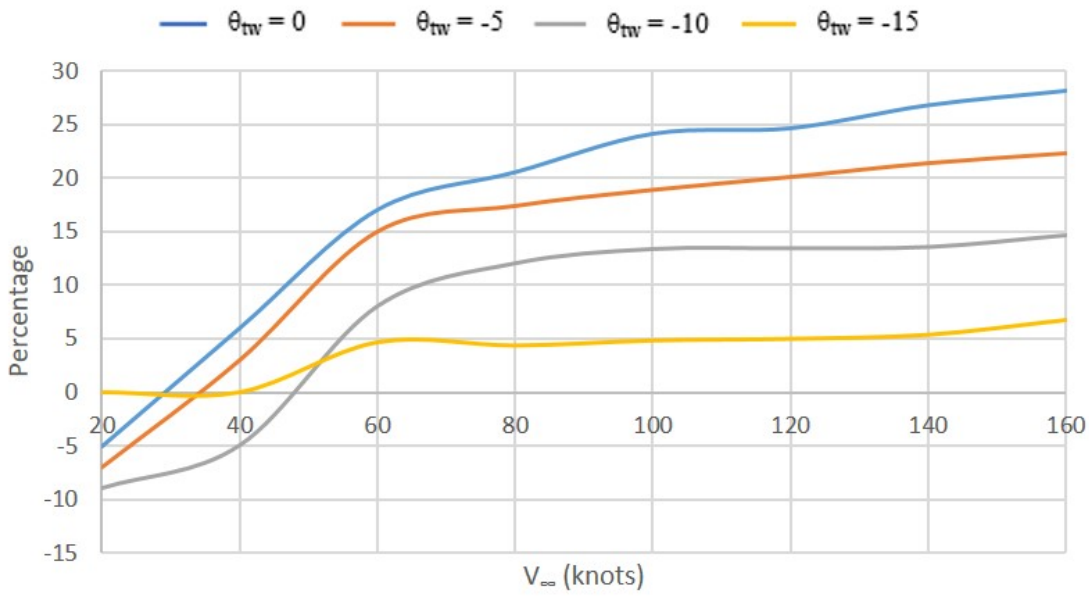

(b) Percent variance from the baseline case

Figure 3.14: Twist effect on rotor drag and variation from the baseline case.

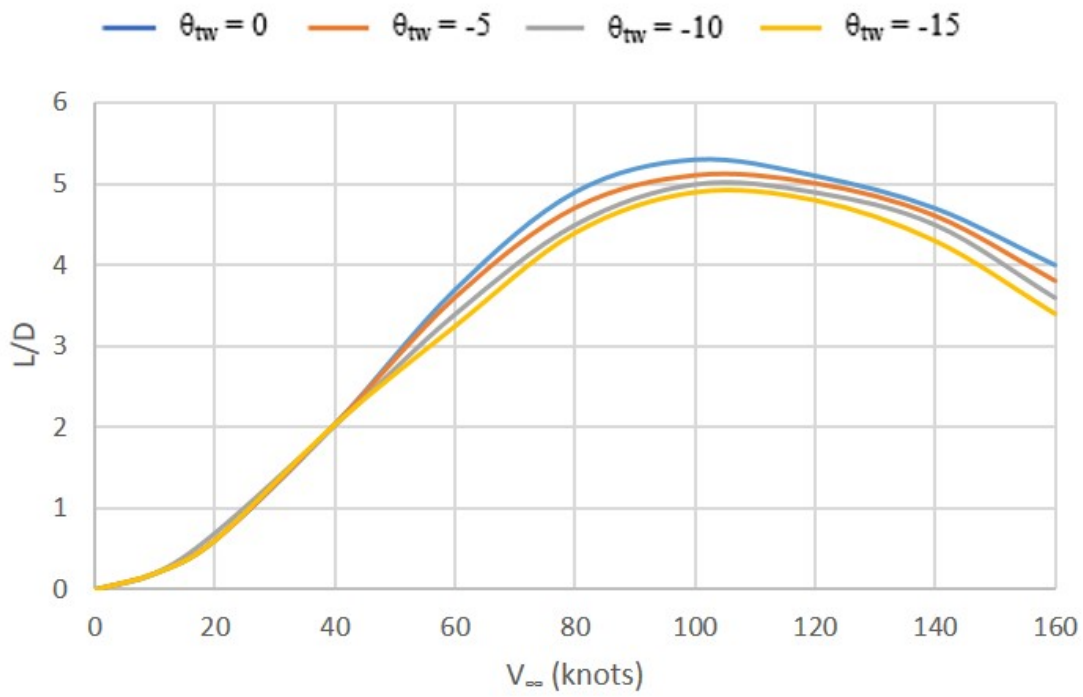

(a) Twist effect on L/D

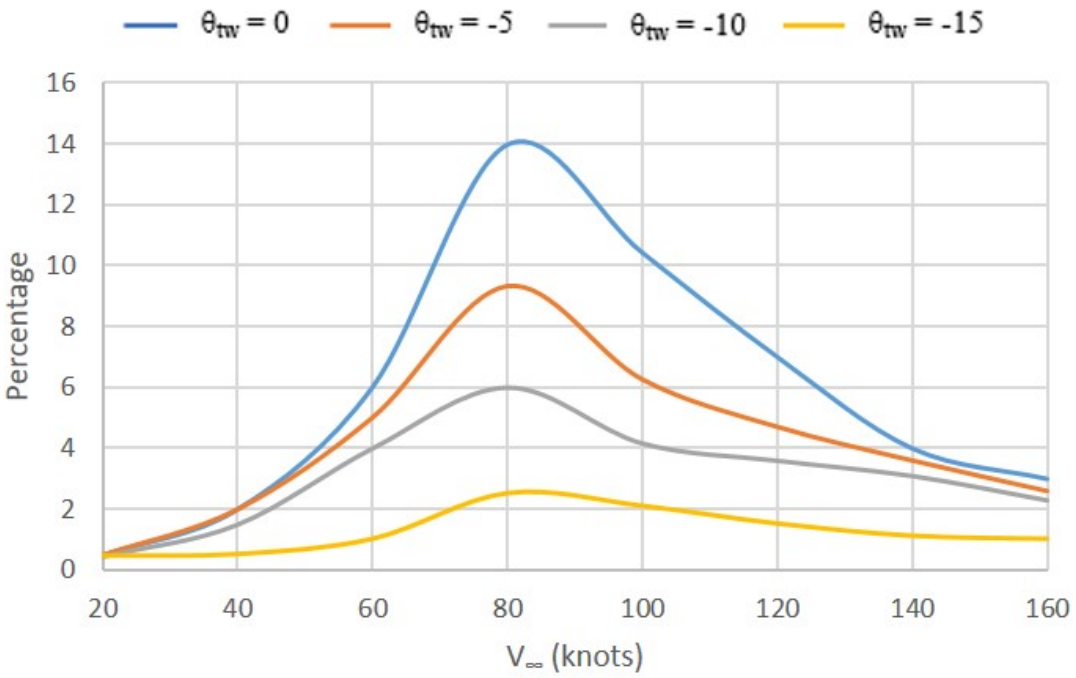

(b) Percent variance from the baseline case

Figure 3.15: Twist effect on L/D and variation from the baseline case.

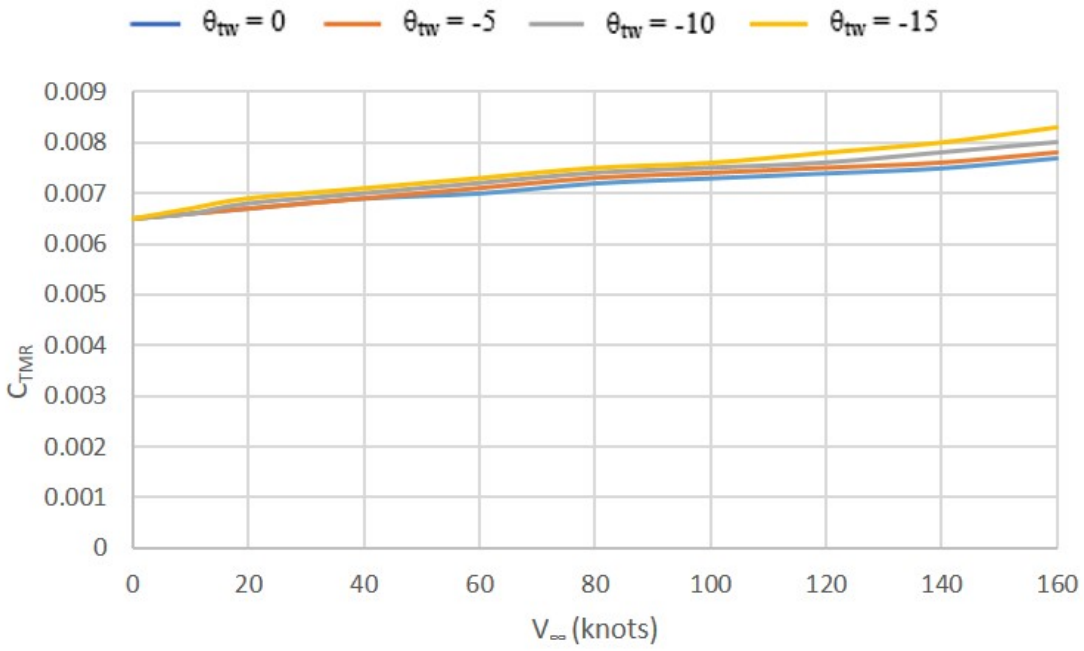

Figure 3.16: Total thrust (C_{TMR}) variation with twist.

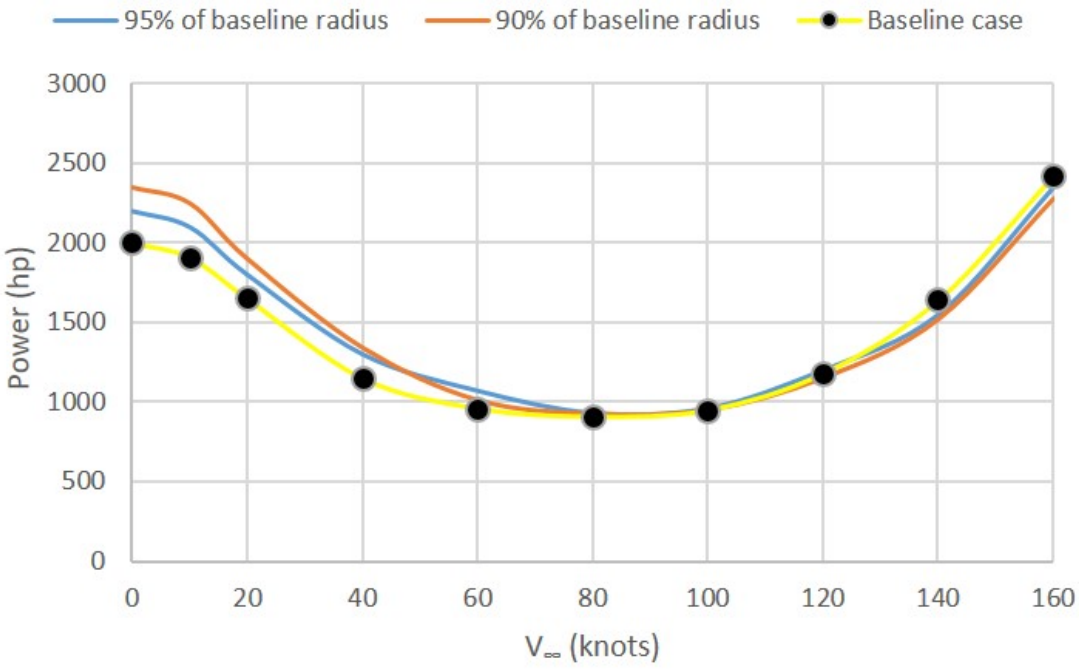

Figure 3.17: Power variation with rotor radius and airspeed.

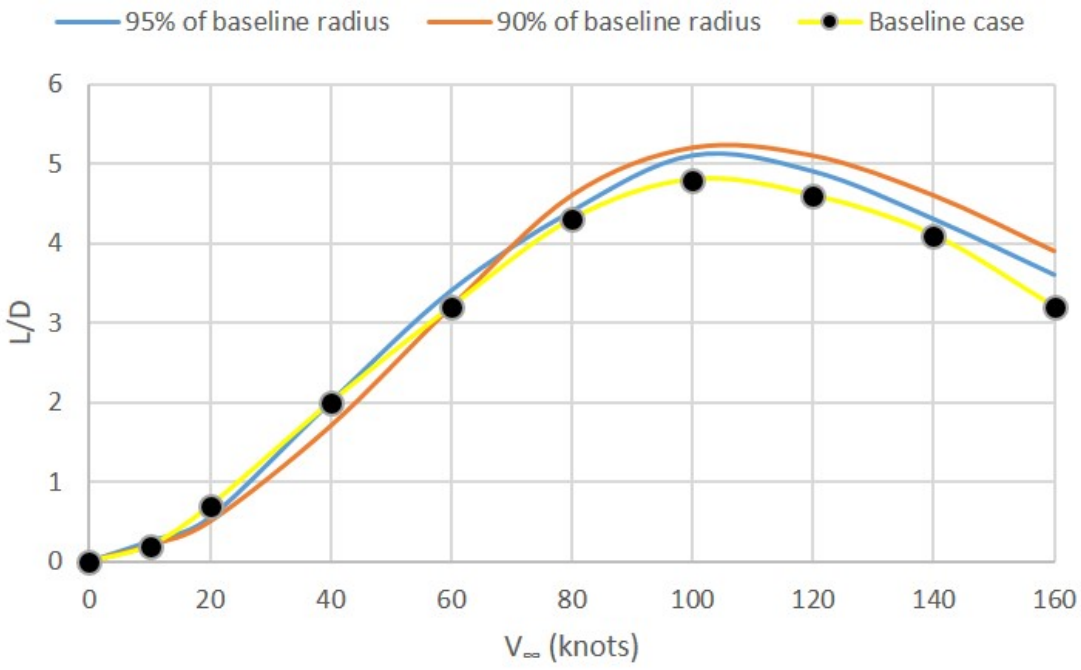

Figure 3.18: L/D variation with rotor radius and airspeed.

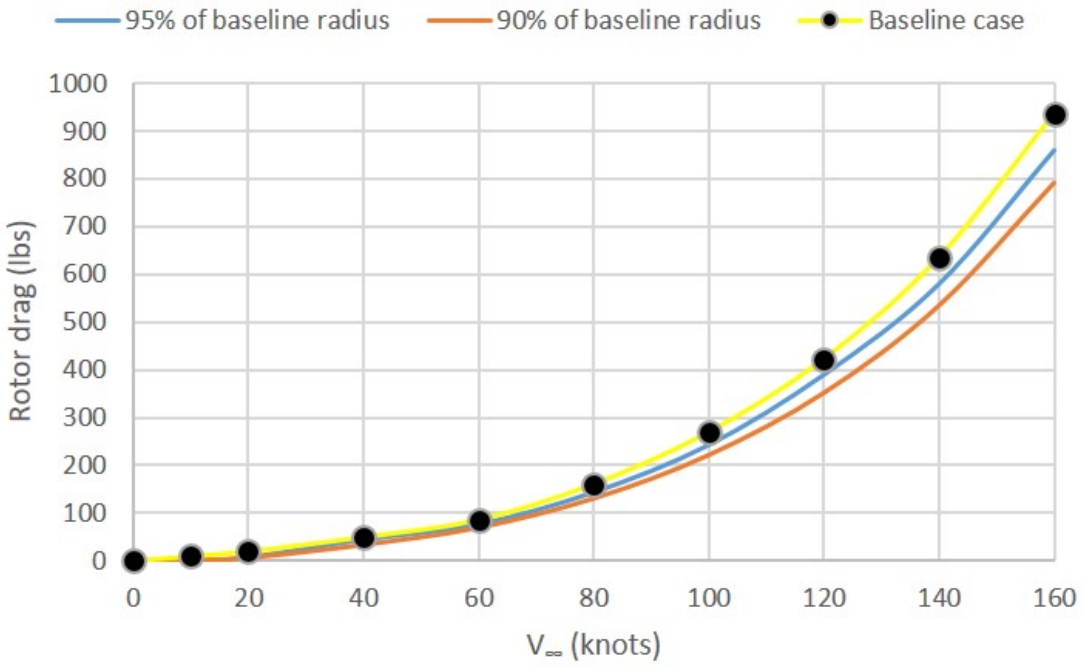

Figure 3.19: Rotor drag variation with rotor radius and airspeed.

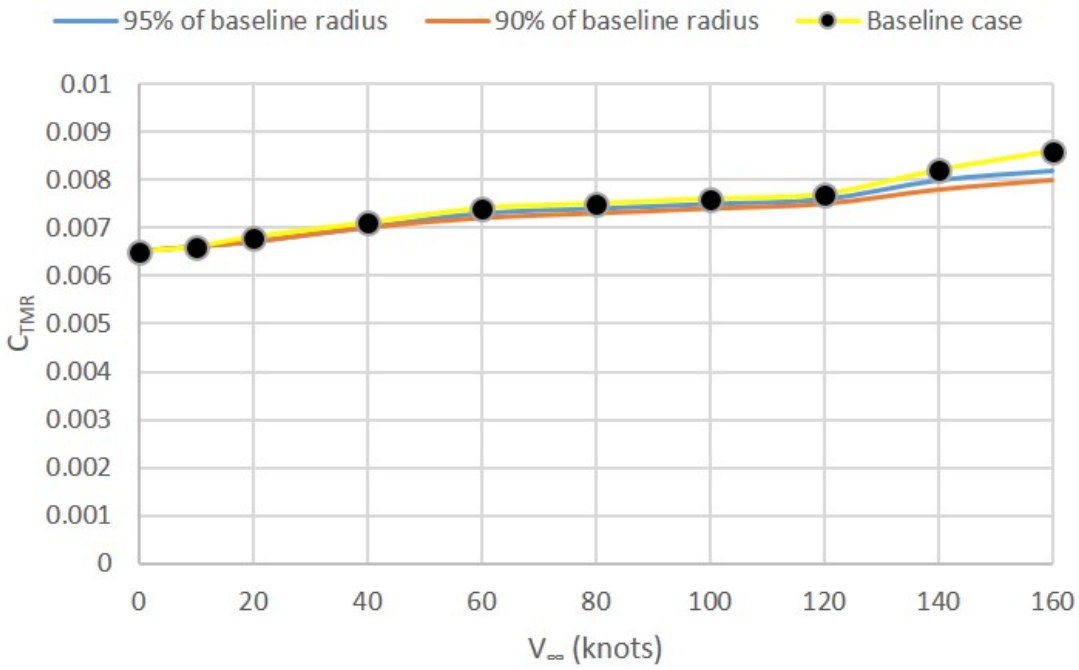

Figure 3.20: Total Thrust (C_{TMR}) variation with rotor radius and airspeed.

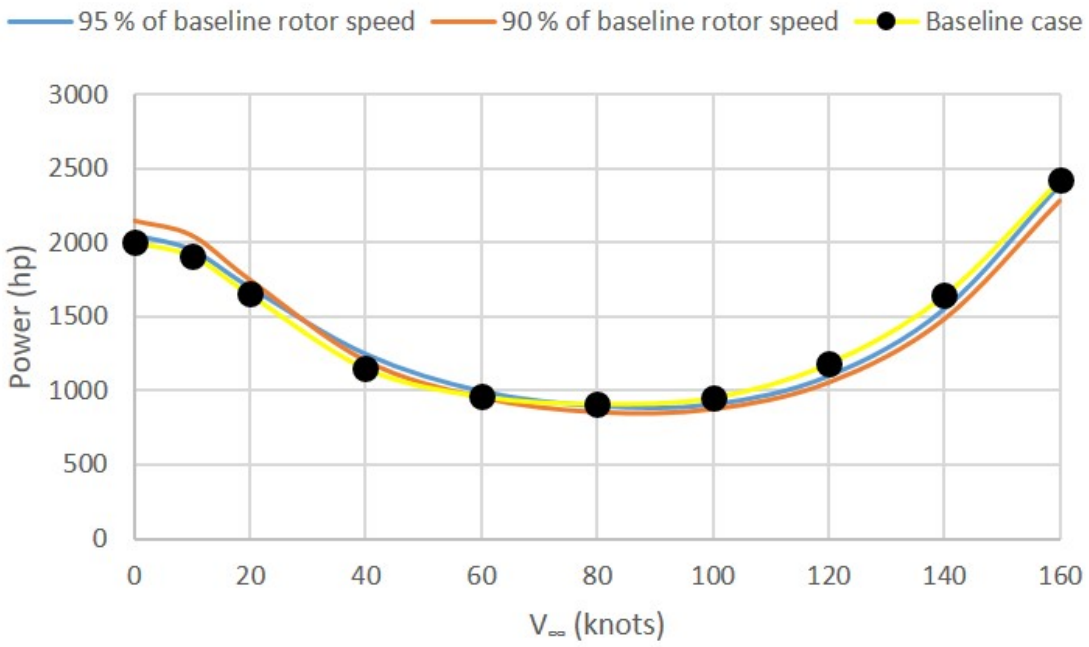

Figure 3.21: Power variation with rotor rpm.

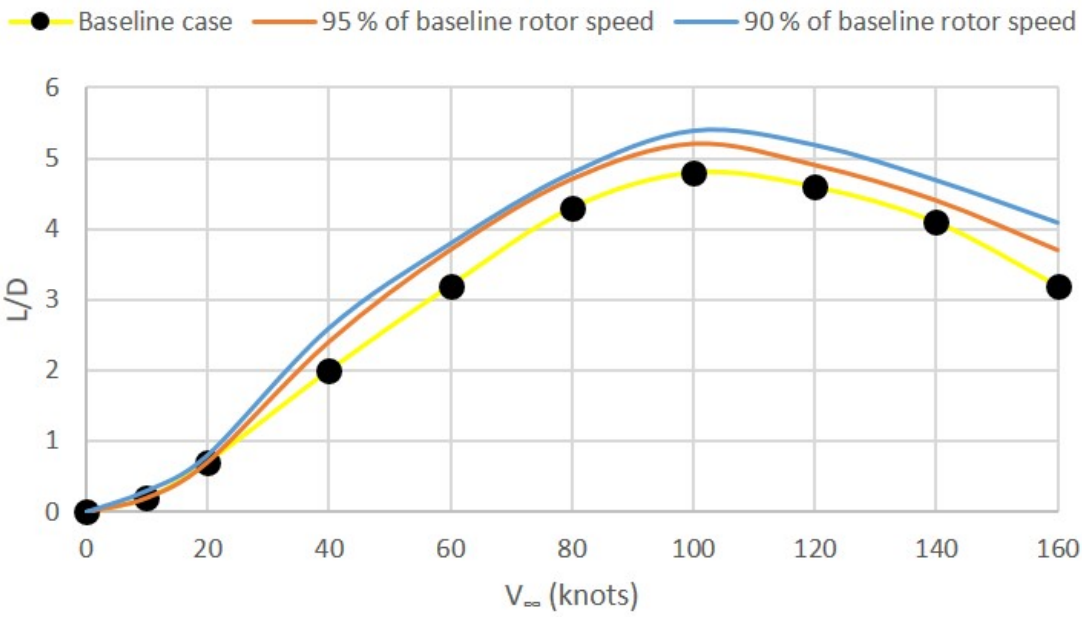

Figure 3.22: L/D variation with rotor rpm.

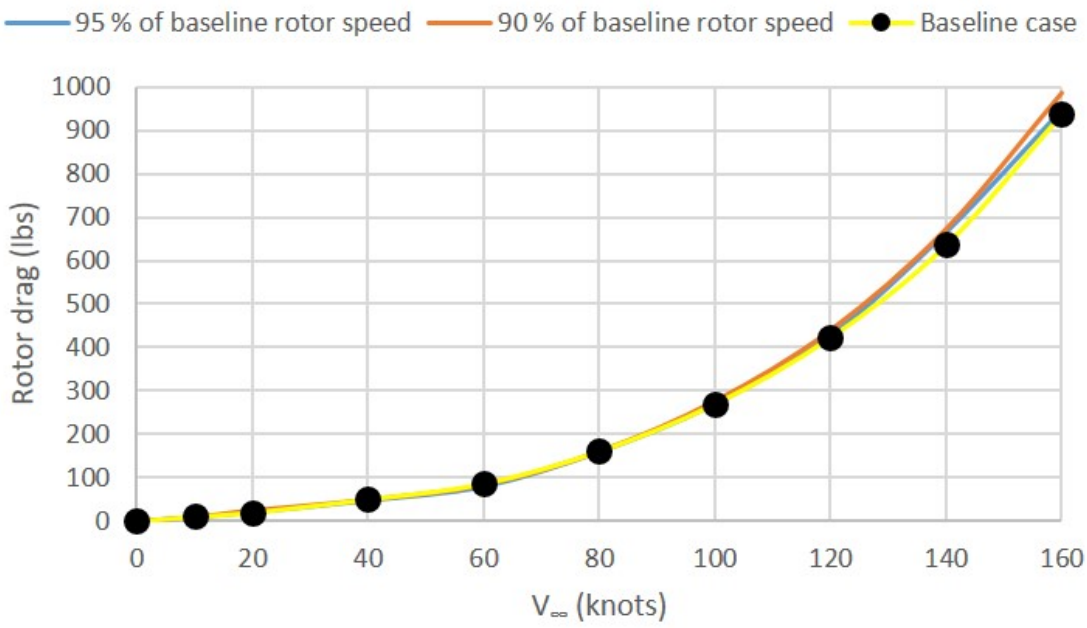

Figure 3.23: Rotor drag variation with rotor rpm.

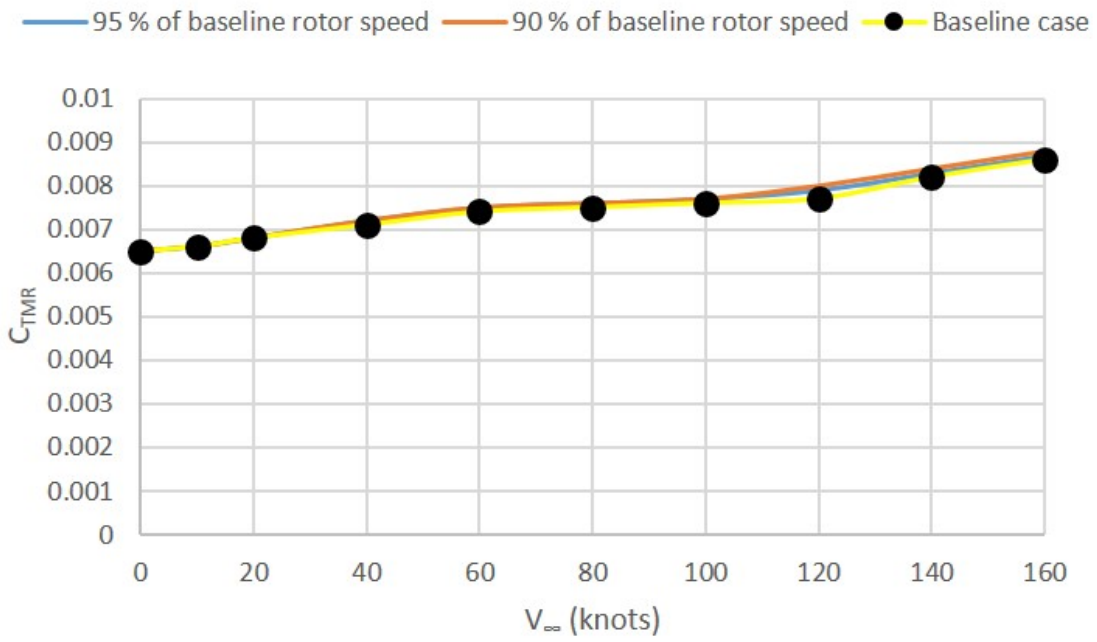

Figure 3.24: Total Thrust (C_{TMR}) variation with rotor rpm.

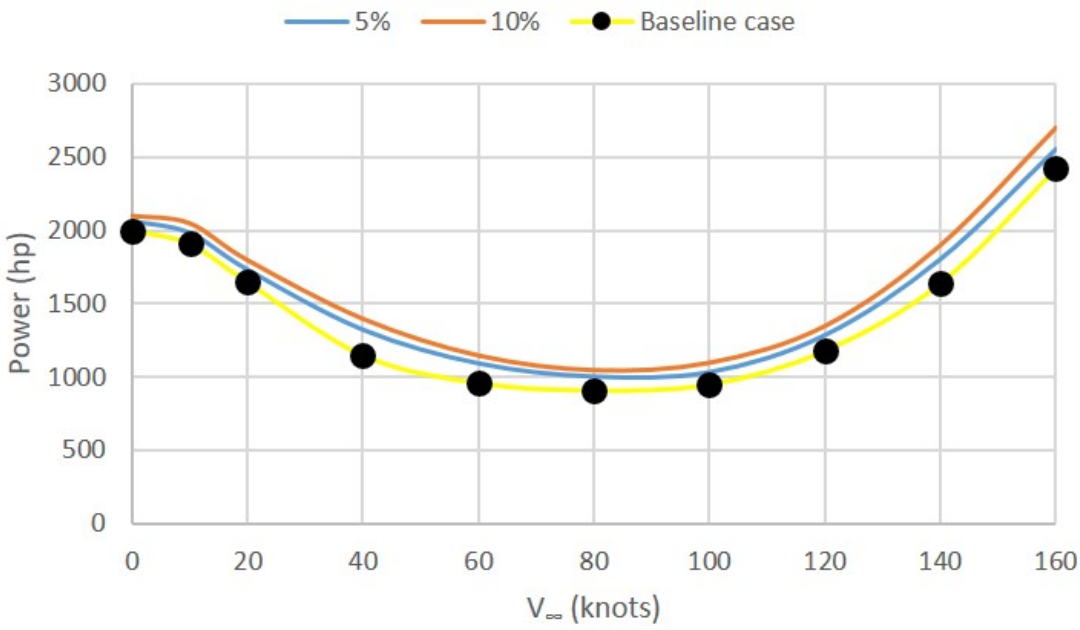

Figure 3.25: Power variation with chord.

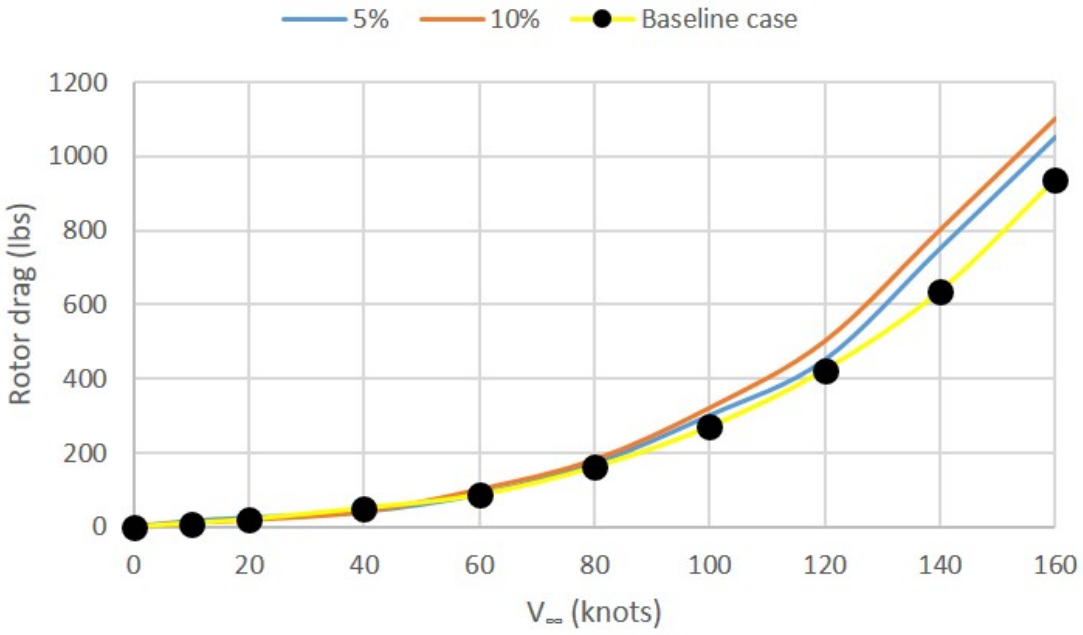

Figure 3.26: Rotor drag variation with chord.

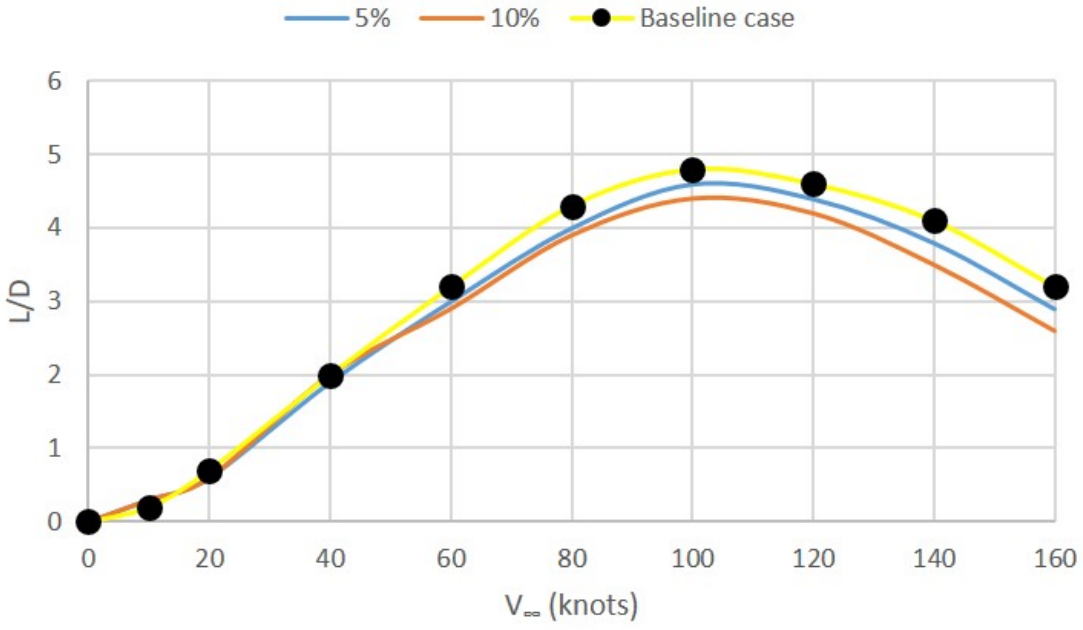

Figure 3.27: L/D variation with chord.

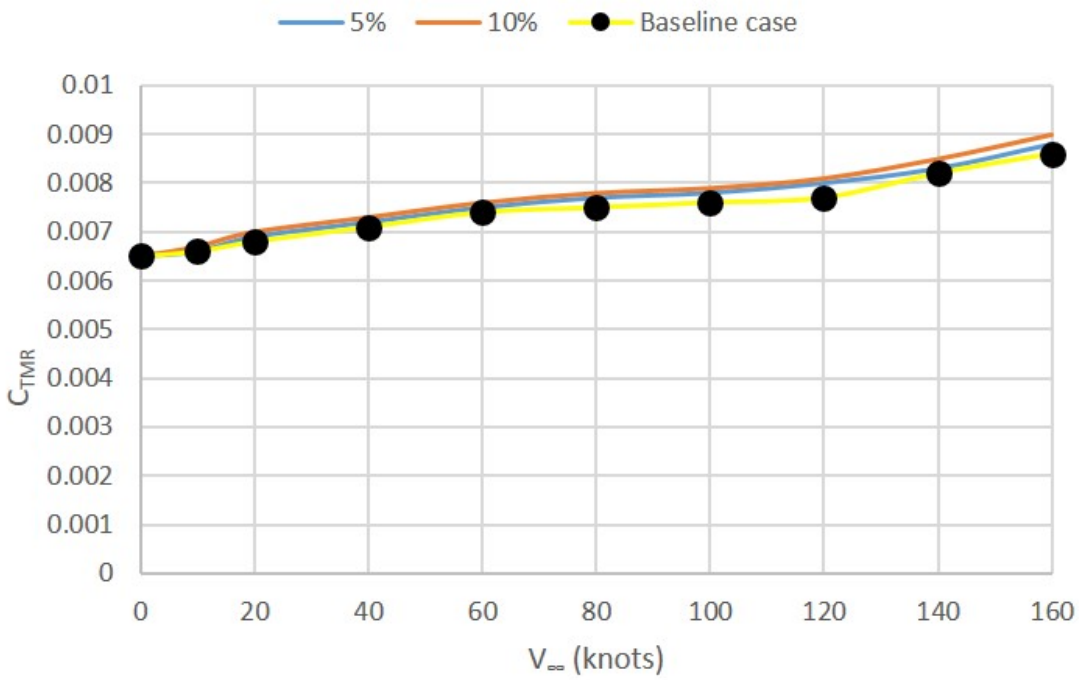

Figure 3.28: Total Thrust (C_{TMR}) variation with chord.

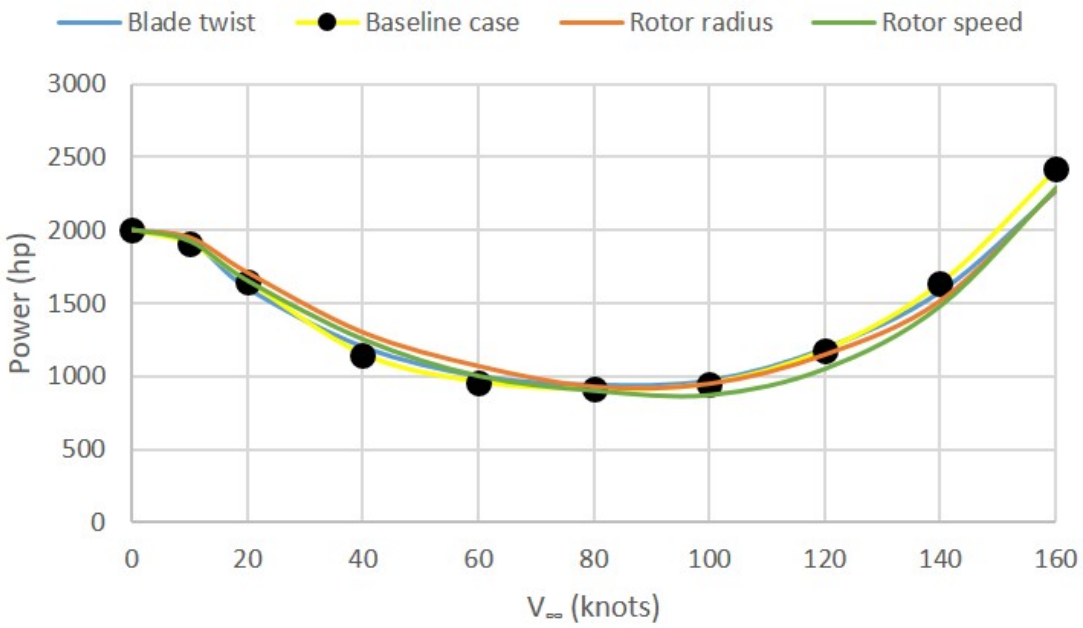

Figure 3.29: Power comparison for a single morphing effect.

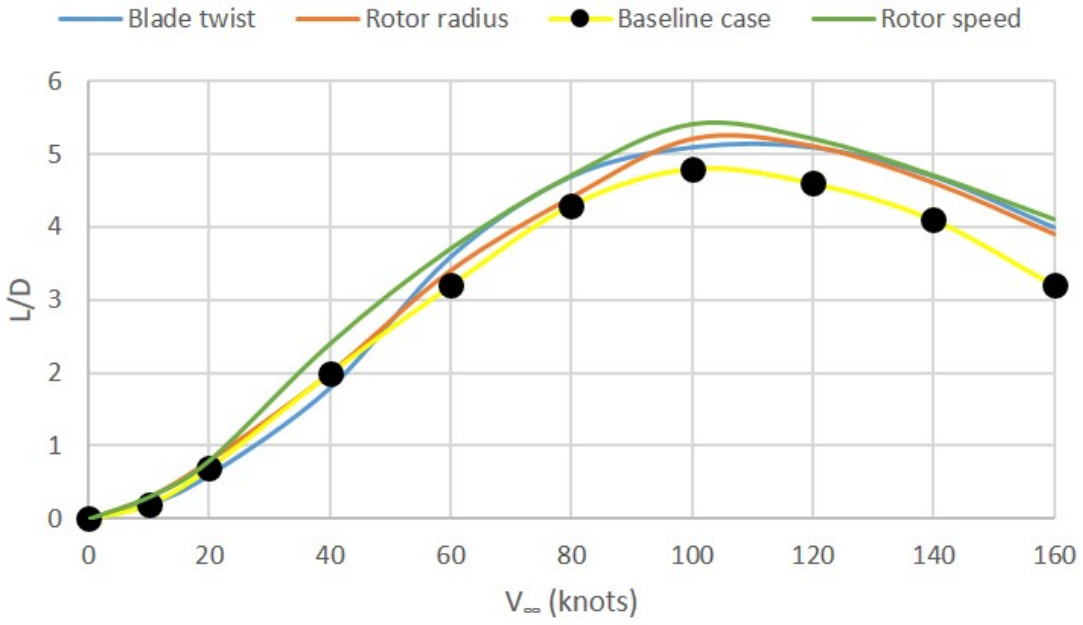

Figure 3.30: L/D comparison for a single morphing effect.

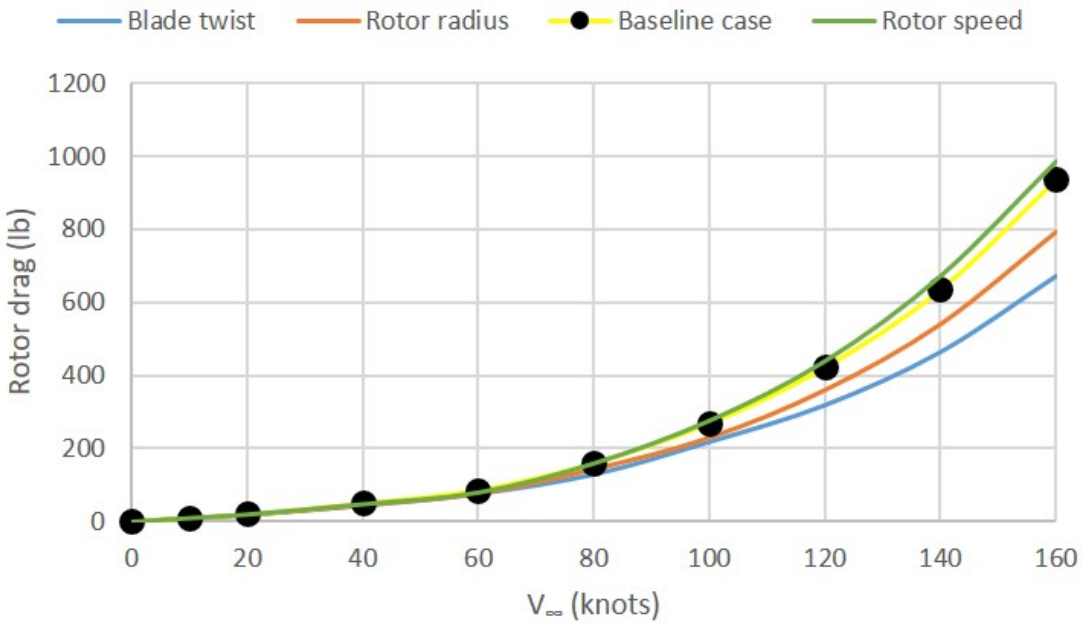

Figure 3.31: Rotor Drag comparison for a single morphing effect.

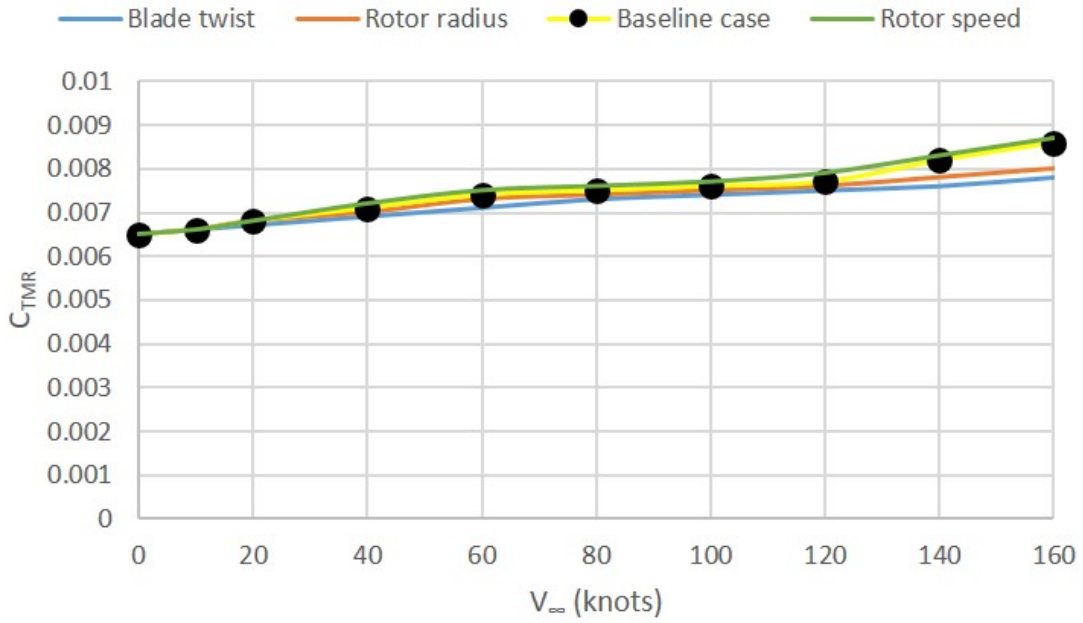

Figure 3.32: Total thrust (C_{TMR}) comparison for a single morphing effect.

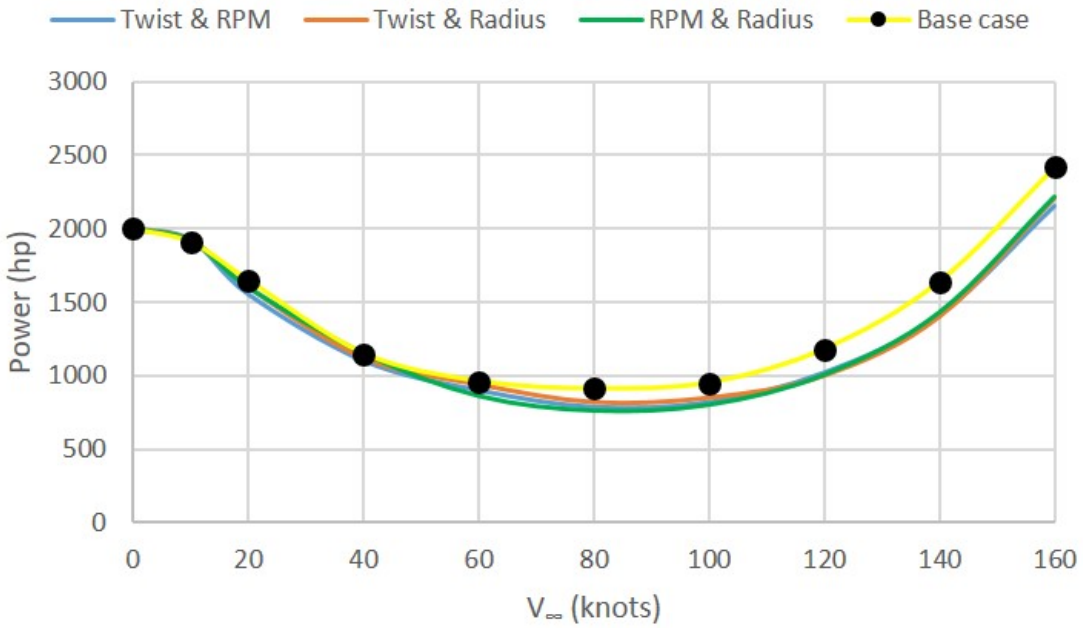

Figure 3.33: Power comparison for two morphing effects.

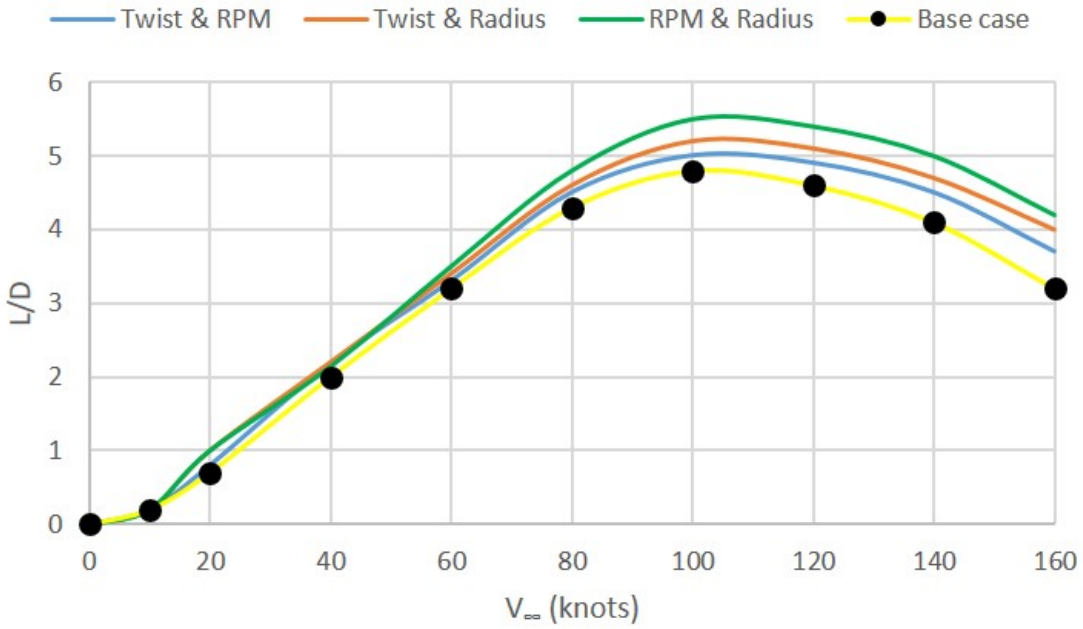

Figure 3.34: L/D comparison for two morphing effects.

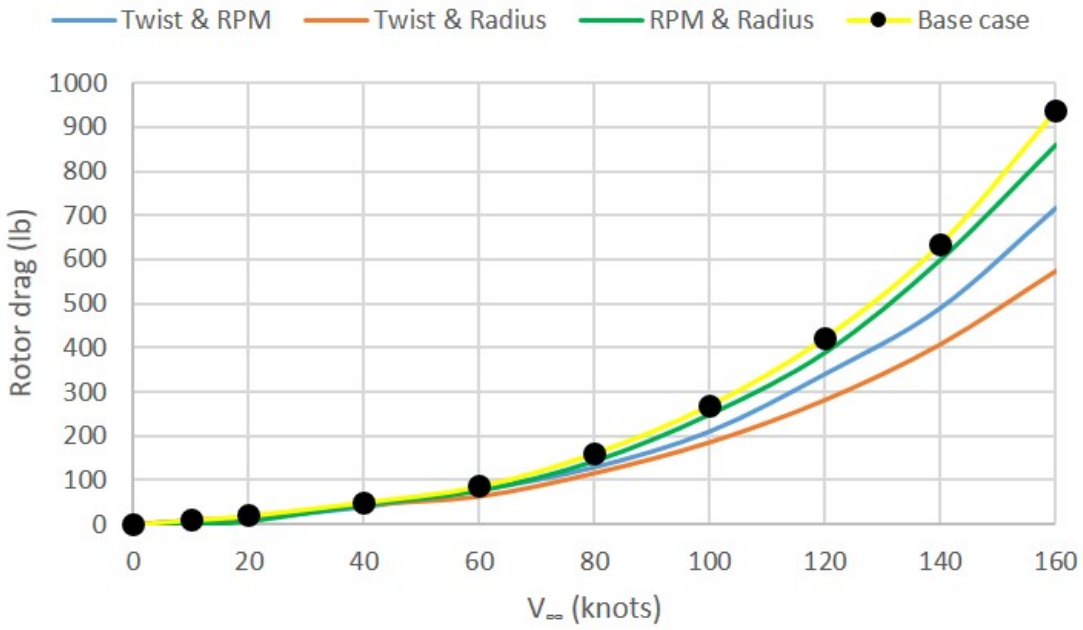

Figure 3.35: Rotor drag comparison for two morphing effects.

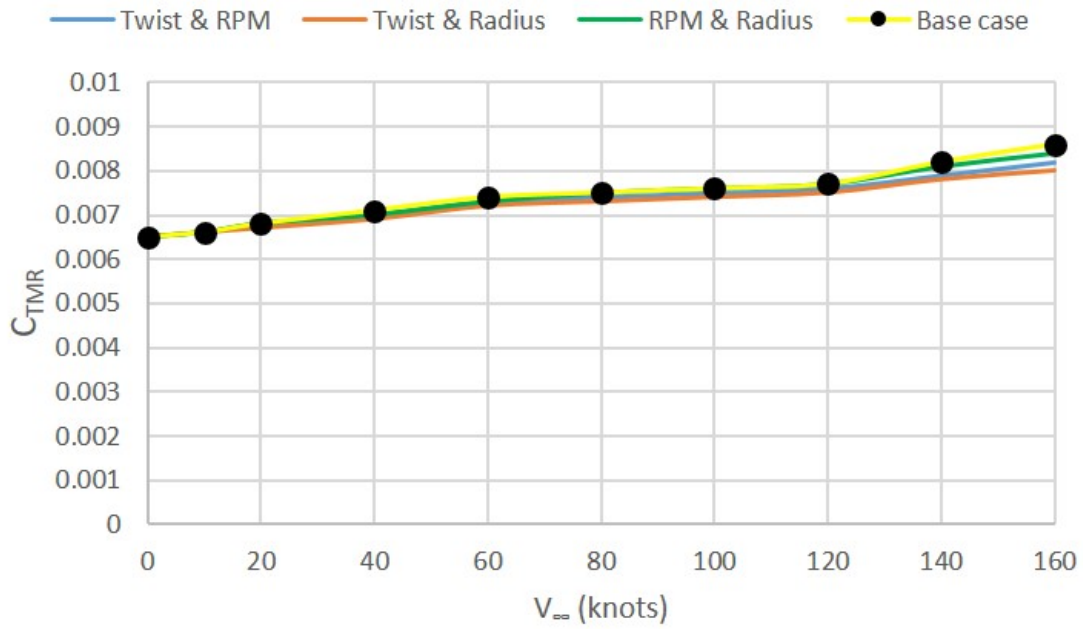

Figure 3.36: Total thrust (C_{TMR}) comparison for two morphing effects.

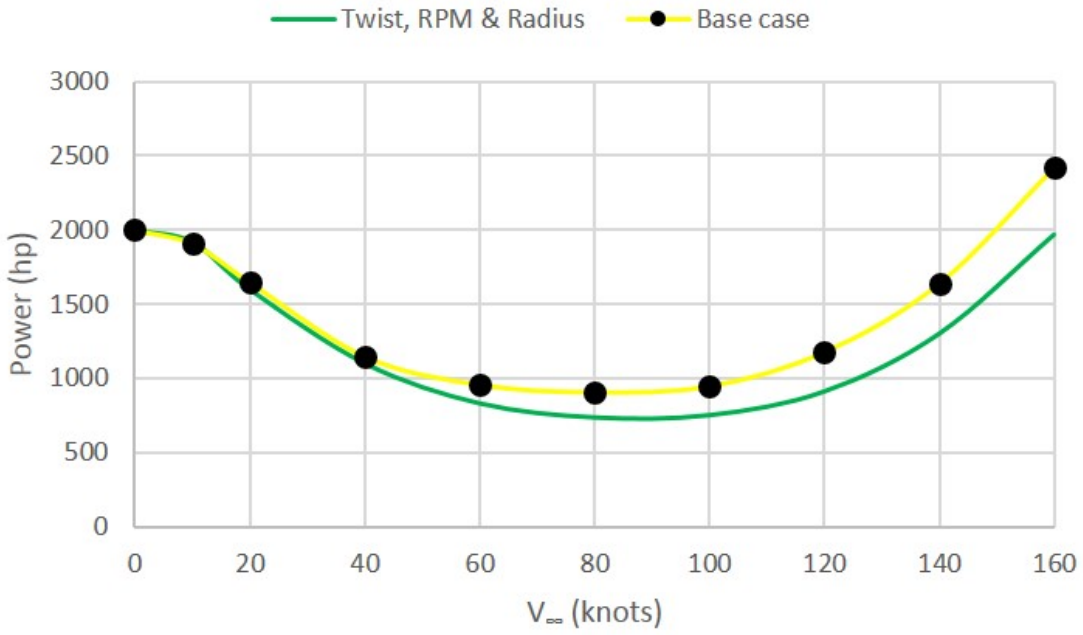

Figure 3.37: Power comparison for all three morphing effects.

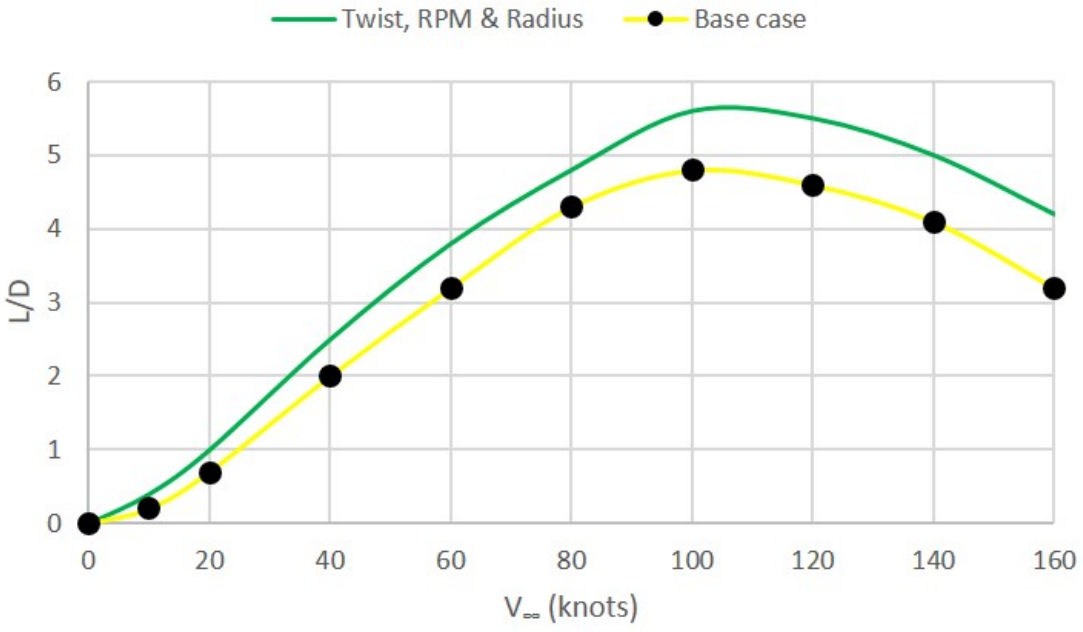

Figure 3.38: L/D comparison for all three morphing effects.

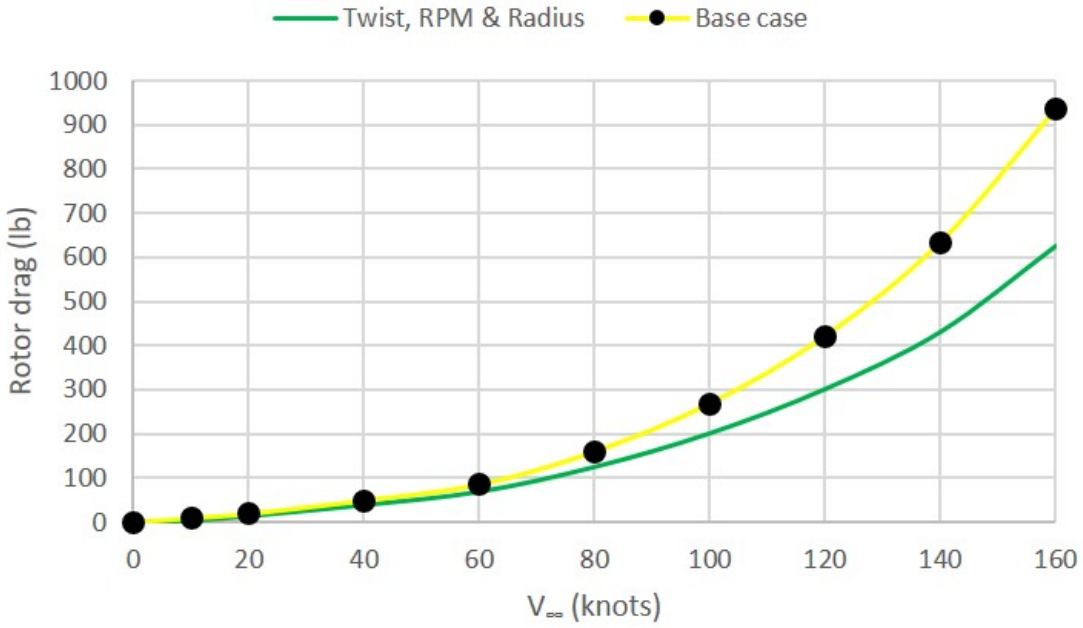

Figure 3.39: Rotor Drag comparison for all three morphing effects.

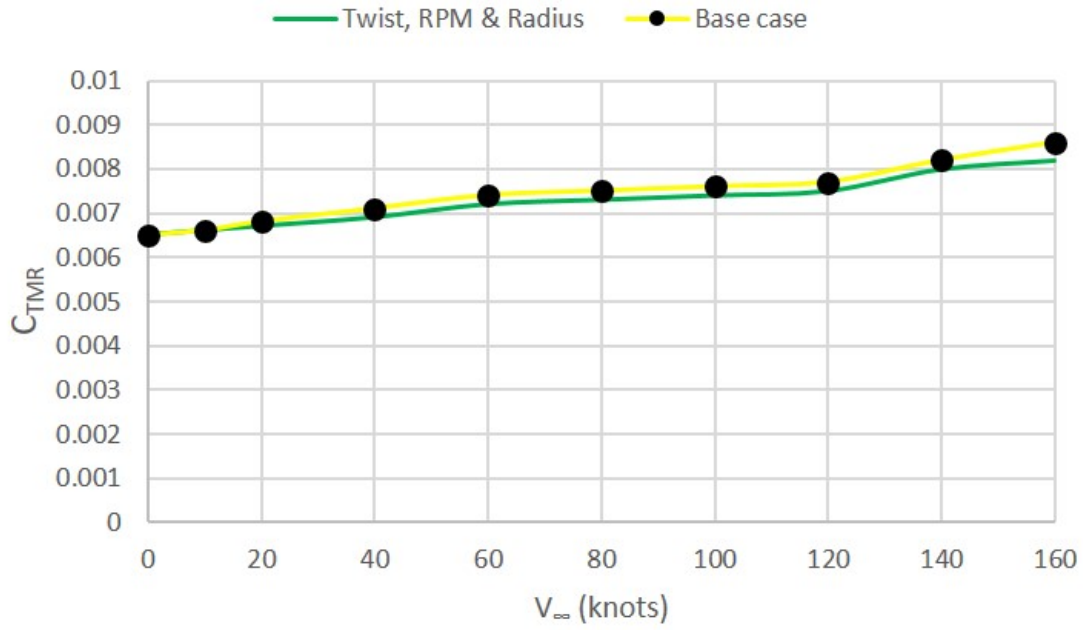

Figure 3.40: Total Thrust (C_{TMR}) comparison for all three morphing effects.

4. Conclusion and Recommendations for Future Work

4.1 Conclusions

The rotor blade element method has been used as a means for analysis in this thesis to examine the potential aerodynamic performance benefits from a morphing rotor system. Only aerodynamic effects were considered with no consideration as to how such morphing might be practically implemented. From the work reported in this thesis, it can be concluded that from an aerodynamic and performance perspective rotor system and/or blade morphing does have some benefits, but those benefits are relatively small. It was found that in some cases the use of morphing would be limited anyway because of other aerodynamic problems that are produced, such as the premature onset of retreating blade stall, compressibility drag rise on the blades, etc.

The following conclusions have been drawn from the work:

1. Higher (negative, nose-down) blade twist was found to maximize hovering performance, while low to moderate blade twist was found to produce lower power requirement and lower rotor drag at higher airspeeds. Little or no blade twist was found to produce the lowest rotor drag at the highest airspeeds. At airspeeds between hover and 60 knots, the effects of blade twist on rotor drag was shown to be very small.

2. On decreasing the rotor radius by up to 10%, the rotor power requirements increased in hover and also at lower airspeeds up to 50 knots, which was because of an increase in rotor disk loading. At airspeeds above 50 knots, decreasing rotor radius begins to reduce the rotor power requirements. Although too much of a reduction in radius results in significantly increased disk loadings and higher power requirements, the blade sections also begin to operate at higher angles of attack on the retreating side of the rotor disk, thereby causing premature blade stall. Decreasing rotor radius decreases rotor drag and, thereby, reduces the propulsive requirements of the rotor system. The lift to drag ratio was also found to increase at higher airspeeds with decrease in rotor radius because of a reduction in rotor drag.

3. Reducing the rotational speed (rpm) of the rotor results in lower power requirements at all airspeeds. But to generate the same total rotor thrust this approach also leads to the blade sections operating at higher angles of attack, so are most likely to stall on the retreating side of the rotor in forward flight. There was a significant increase in the rotor lift to drag ratio at moderate and higher airspeeds, with a maximum gain of 0.6 at 100 knots when reducing rotor speed by 10%.

4. Although Khoshlajeh and Gandhi [Ref. 29] have conducted research into a "morphing chord" blade by using part-span extendable flaps at moderate and higher airspeeds and have claimed modest rotor performance improvements, the area increase from a flap is smaller compared to increasing the entire blade chord. It was shown in this thesis that any increase in blade chord leads just leads to higher rotor drag

because of higher blade area, the upshot being an increase in power requirements at any airspeed and also a decrease in rotor lift to drag ratio in forward flight.

5. Changing blade twist was found to provide the most power reductions at lower airspeeds while reducing rpm provided the most gains at moderate and higher airspeeds. Lift to drag ratio decreased at all airspeeds with a maximum gain of 0.75 at 100 knots obtained from varying rotor rpm. A blade twist reduction from the hover value provided a power saving of 150 hp at 160 knots, but this is equivalent only to about a 67 lb/hr fuel savings. For a flight of 2 hours, 135 lbs of fuel is saved and hence flight time could only be extended by a modest 8 minutes.

6. Morphing of the rotor was carried out by systematically varying blade twist, blade radius and rotor rpm as a function of airspeed. Blade twist was changed such that it was -18° in hover to 0° at 160 knots, rpm was varied such that it was 100% at hover to 90% at 160 knots, and rotor radius was changed such that it was 100% in hover to 90% at 160 knots. On morphing two effects simultaneously, power gains were found to be more significant compared to morphing single effects. At low airspeeds, morphing blade twist and rotor rpm provided the most benefits while at moderate airspeeds of 50–110 knots, varying rotor rpm and blade radius offer the most benefits. At higher airspeeds, morphing blade twist and rotor radius together gave the most gains in performance. Reducing both rpm and radius at 160 knots gave a 300 hp reduction in power and approximately 135 lb/hr of fuel savings.

7. Reducing blade twist and radius simultaneously leads to more drag reductions at all airspeeds than other forms of morphing, with a maximum drag reduction of 370 lb at 160 knots. The lift to drag ratio was shown to increase for these cases over the baseline rotor. Varying blade twist, rotor rpm and blade radius simultaneously gives the maximum power reductions possible at all airspeeds when compared to all other morphing cases. A maximum power reduction of 420 hp was attained at 160 knots, which results in fuel savings of 189 lb/hr and total fuel saving of 378 lbs over a 2 hour flight. A fuel savings of 378 pounds is equivalent to an extra flight time of about 21 minutes.

From above conclusions, it can be seen that the maximum extra flight endurance that could be obtained by morphing a rotor is around 5–15 minutes for all cases except the one where twist, radius and rpm are all morphed. While even an extra 10 minutes could be critical to certain flight missions, the work in this thesis ignores all of the other penalties incurred by "morphing" a blade or a rotor system. For instance, morphing twist, radius and rpm offers benefits at higher speeds and modestly increased flight time but each morphing system requires its own actuators and combining three such systems would make the rotor system very heavy. This could obviously offset any benefits.

4.2 Recommendations for Future Work

In terms of future work, it would be worthwhile to analyze other combinations of rotor and blade morphing with respect to airspeed. Another factor that could be considered

is to morph the blade as a function of blade azimuth location because helicopter blade operates very differently on the retreating and advancing sides of the rotor disk. However, it is recognized that morphing the blade as a function of time may be very challenging in practice. Furthermore, it would be interesting to investigate morphing from a structural and weight perspective and analyze the impact of adding such systems to a rotor blade. Also, analyzing the aspect of reliability, maintenance and certification of such systems would be critical to understanding the practical feasibility of morphing blades and morphing rotors, in general. Even if such morphing was to be aerodynamically useful and even practical, there would still have to be further studies on the effects of morphing on vibrations and noise. Most helicopters have high amounts of vibrations and noise, so if morphing reduces vibrations and acoustics significantly then it might prove advantageous even if only small performance benefits are realized.

Bibliography

[1] aviastar, "Vought-Sikorsky VS-300," 2016. [Online]. Available: www.aviastar.org

[2] SSGT Suzanne M Jenkins USAF, "UH-60L Blackhawk helicopter flies a low-level mission over Iraq," 2004. [Online]. Available: Defenseimagery.mil, VIRIN 040107-F-9629J-009

[3] J Gordon Leishman, *Fundamentals of Helicopter Aerodynamics*. Cambridge University Press, 2006.

[4] Franchesca Fusi, Guiseppe Quaranta, Alberto Guardone and Pietro Congedo, "Robust aerodynamic optimization of morphing airfoils for helicopter rotor blades," *AIAA*, 2015.

[5] Hong Jie Tseng and Wei Cheng Tian and Wen Jong Wu, "Flexible PZT Thin Film Tactile Sensor for Biomedical Monitoring," *Sensors(Basel)*, pp. 5478–5492, 2013.

[6] Cassio T Faria and Alexander M. Pankonien and Daniel J. Inman, "Synergistic Smart Morphing Aileron," 2013.

[7] Daniel J. Fernandes and Rafael V. Peres and Alvaro M. Mendes and Carlos N. Elias, "Understanding the Shape Memory Alloys used in Orthodontics," *ISRN Dentistry*, 2011.

[8] DJ Lee and HC Kim and BG Min , "Development of a new blood pump using a shape memory alloy actuator," *ASAIO Journal*, pp. 765–768.

[9] Justin K. Strelec and Dimitris C. Lagoudas and Mohammad A. Khan and John Yen , "Design and Implementation of a Shape Memory Allow Actuated Reconfigurable Airfoil," *Journal of Intelligent Material Systems and Structures*, 2003.

[10] Jeanette J. Epps and Inderjit Chopra, "In Flight Tracking of Helicopter Rotor Blades using Shape memory alloy actuators," *AIAA*, 1999.

[11] Nirmit Prabhakar, "Design and Dynamic Analysis of a variable sweep, variable span morphing UAV," 2014.

[12] Zhang Haibo and yan Changkai and Chen Guoqiang, "Variable rotor speed control for an integrated helicopter/engine system," *Journal of Aerospace Engineering*, pp. 323–341, 2013.

[13] NASA, "A Sequential Shifting Algorithm for Variable Rotor Speed Control," 2007.

[14] Lidia M. Belmonte and Rafael Morales and Antonio Fernandez-Caballero and Jose A. Somolinos, "A Tandem Active Disturbance Rejection Control for a Laboratory Helicopter With Variable-Speed Rotors," *IEEE*, pp. 6395–6406, 2016.

[15] Benjamin K.S Woods and M Senthil Murugan and Michael I Friswell, "Morphing Helicopter Rotor Blade with Curvilinear Fiber Composites," *European Rotorcraft Forum*, 2012.

[16] Dong Han and Edward Smith, "Lagwise dynamic analysis of a variable speed rotor," *Aerospace Science and Technology*, pp. 277–286, 2013.

[17] Peter C Chen and Inderjit Chopra, "Wind tunnel test of a smart rotor with individual blade twist control," *SPIE*, pp. 217–230, 1997.

[18] A. Staino and B. Basu, "Dynamics and Control of vibrations in wind turbines with variable rotor speed," *Engineering Structures*, pp. 58–67.

[19] Dong Han and Joseph Wang and Edward C. Smith and George A. Lesieutre, "Transient Loads Control of a Variable Speed Rotor during Lagwise Resonance Crossing," *AIAA*, pp. 20–29, 2013.

[20] Harsha Prahlad and Inderjit Chopra, "Design of a variable twist tilt rotor blade using shape memory alloy (SMA) actuators," *SPIE*, pp. 46–59, 2001.

[21] R. M. Ajaj and M. Bourcha and W. Harsani, "Twist Morphing Using the Variable Cross Section Spar: Feasibility Study," *Journal of Aerospace Engineering*, 2015.

[22] Phuriwat Anusonti-Inthra and Robert Sarjeant and Mary Frecker and Farhan Gandhi, "Design of a Conformable Rotor Airfoil Using Distributed Piezoelectric Actuators," *AIAA*, pp. 1684–1695, 2005.

[23] F. Gandhi, "Variable chord morphing helicopter rotor," Patent, 2014.

[24] Mestrinho, J., Gamboa, P., Santos, P., "Design Optimization of a Variable Span Morphing Wing for a Small UAV," *AIAA/ASME/AHS Structures, Structural Dynamics and Materials Conference*, 2011.

[25] M Secanell and A Suleman and P Gamboa, "Design of a Morphing airfoil using aerodynamic shape optimization," *AIAA*, pp. 1550–1562, 2006.

[26] Gianluigi Alberto Miste and Ernesto Benini, "Variable Speed Rotor Helicopters: Performance Comparison Between Continuously Variable and Fixed Ratio Transmissions," *AIAA*, pp. 1189–1200, 2016.

[27] Analytical Methods, "MSES/MISES," 2016. [Online]. Available: http://www.ami.aero/software-computing/

[28] David Matuska and Allen Dale and Peter Lorber, "Wind Tunnel Test of a Variable-Diameter Tiltrotor (VDTR) Model," 1994.

[29] Maryam Khoshlahjeh, "Extendable chord rotors for helicopter performance improvement and envelope expansion," Pennsylvania State University, 2012.

[30] Mihir Mistry and Farhan Gandhi, "Helicopter Performance Improvement with Variable Rotor Radius and RPM," *Journal of American Helicopter Society*, pp. 17–35, 2014.

[31] Robert Porter and Biajn Shirinzadeh and Man Ho Choi, "Experimental Analysis of Variable Collective-pitch Rotor Systems for Multirotor Helicopter Applications," *Journal of Intelligent and Robotic Systems*, pp. 271–288, 2016.

[32] Inderjit Chopra, "Aeromechanics of an Optimized, Actively-Morphing Rotor System," 2013.

[33] George N Barakos and Dong Han and Vasileios Pastrikakis, “Helicopter Performance Improvement by Variable Rotor Speed and Variable Blade Twist,” *Aerospace Science and Technology*, pp. 164–173, 2015.

[34] Verticalmag, “Bell Helicopter unveils futuristic FCX-001 concept aircraft,” 2017. [Online]. Available: https://www.verticalmag.com/news/bell-helicopter-unveils-futuristic-fcx-001-concept-aircraft/

[35] William G. Bousman, *Aerodynamic Characteristics of SC1095 and SC1094R8 airfoils*. NASA, 2003.

[36] Tools Airfoil, “SC1095 data,” 2017. [Online]. Available: airfoiltools.com

[37] MATLAB, “Solve nonstiff differential equations medium order method, ODE45 ,” 2016. [Online]. Available: https://www.mathworks.com/help/matlab/ref/ode45.html

[38] University of Bristol, “Cruise Performance,” 2004. [Online]. Available: https://www.southampton.ac.uk

[39] “UH-60A/L Black Hawk Helicopter,” 2004. [Online]. Available: http://www.military.com/equipment/uh-60a-l-black-hawk

[40] Minnesota National Guard, *UH-60 Black Hawk*, 2004. [Online]. Available: http://www.minnesotanationalguard.org/units/assets/equipment/Blackhawk.pdf

A. Appendix: Main MATLAB Code

```
% Main Rotor code


clc;

clear;


run('Constants.m')

Vinf = 0 *1.68781; % ft/sec (0 for hover)

tot_deg =  1 * 360; % number of revolutions

alpha_tpp = 0 *0.01745;

rev = 1 * 36; % number of total sections


while Ct_req > Ct && beta_1s <= 0.2 && beta_1c <= 0.1


 if abs(Ct-Ct_req) > 0.0001

 twisto = twisto + 0.1*0.01745;

 else

 twisto = twisto - 0.01*0.1745;

 end
```

```
 if beta_1s > 0.2
  pitch1c = pitch1c + 0.1*0.01745;
 else
  pitch1c = pitch1c - 0.1*0.01745;
 end

 if beta_1c > 0.2
  pitch1s = pitch1s - 0.1*0.01745;
 else
  pitch1s = pitch1s + 0.1*0.01745;
 end

for count = 1:(rev)

 angle_prev = angle;
 angle = ((tot_deg/rev)*count);
 angle_plot(:,count) = angle ;
 psi = (angle) *0.01745; % psi in radians
 dpsi = tot_deg/rev;

 for i = 1:(n-1)
```

```
% Blade Geometry
y = (R/n) * i ; % y
y1(:,i) = y;
c = 1.73; % chord at segment (ft)
c_save(:,i) = c;
% pitch1s = 0 /57.3;
% pitch1c = 0 /57.3;
advance = (Vinf*cos(alpha_tpp))/Vtip;

% Solidity
sigma = (Nb*c)/(pi*R);
%sigma = 3*sigma_eq*r*r*dr;
sigma1(:,i) = sigma;
%theta_tip = 4/57.3;
theta = twisto + twist_rate * y + pitch1s * sin(psi) + pitch1c * cos(
%theta = theta_tip/r; % hyperbolic twist
theta_save(:,i) = theta;

% Compressibility effects
V_element = (Vtip/R)*y; % Element velocity
ut = V_element + Vtip*advance *sin(psi);
```

```
Minf = ut/1117;
cla = 2*pi/(sqrt(1- Minf^2)) ; % 1/radians


%Inflow
 while error_inflow > 0.5
lamda_avg = (advance * tan(alpha_tpp)) + ((Ct)/(2* sqrt(advance*advan
F = 1; % Assume F for initial iteration
ff = 1;
for inflow_iter = 1:10
ff = (Nb/2)*((R - y)/phi*y);
F = (2/pi)* (acos(exp(-ff)));
end
lamda_avg = lamda_avg/F;
error_inflow = abs((lamda_avg - lamda_avg_prev)/lamda_avg );
if i>1
   lamda_avg_prev = lamda1(:,i-1);
end
end


chi = atan(advance/lamda_avg);
kx = tan(chi/2)
ky = 0;
```

```
lamda = lamda_avg*(1+ kx*y*cos(psi) + ky*y*sin(psi));


lamda1(:,i) = lamda;


% Lift Coeff
up = lamda*Vtip + (beta_dot * y);
pt = up/ut;
phi = atan(pt);
alpha = theta - phi;
alpha1(:,i)= alpha ;
Cl = cla*(alpha - (-0.7 /57.3));
Cl1(:,i) = (Cl);


 if Cl > 1.5 && y > e*R
    fprintf('Compressiblity Cl!')
    disp(Cl)
    disp(angle)
    disp(y)
    pause
 end


% Drag From excel
```

```
cdo = 0.007;

d1 = -0.0002;

d2 = 0.0002;

dcd = cdo + alpha*d1 + alpha*alpha*d2;

if ut<=0

    dcd = 3*dcd;

end


if Minf > 0.8

   dcd = dcd + 12.5*(Minf - 0.8)^3;

end


dcd_save(:,i) = dcd;


% Thrust & mb

dy = R/n ;

u = sqrt(ut^2 + up^2);

delta_lift = 0.5 * rho * u * u * c * Cl * dy ;

lift_save(:,i) = delta_lift;

delta_mb = (1 /(rho * cla * c * Vtip * Vtip * R * R)) * (delta_lift *

delta_drag = 0.5 * rho * u * u * c * dcd * dy;

dmb_save(:,i) = delta_mb;
```

```
dthrust = delta_lift*cos(phi) - delta_drag*sin(phi);
dthrust_save (:,i) = dthrust;
dPi = delta_lift*sin(phi)*V_element;
dPi_save(:,i) = dPi;
dPo = delta_drag*cos(phi)*V_element;
dPo_save(:,i) = dPo;

end

% Blade Flapping
lock = 8; %(rho * cla * c * (R^4))/Ib ;
mb = trapz(dmb_save);
vb = sqrt(1 + ((3*e)/(2*(1-e))));
prev_time = count-1;

save('Main_code', 'vb');
save('Main_code', 'lock');
save('Main_code','mb');

if count == 1
    [tt,b] = ode45(@flap, [ angle_prev angle], [0*0.01745 0] );
else
```

```
        [tt,b] = ode45(@flap, [ angle_prev angle], [beta 0] );
    end


    beta_dot = (b(end,2)); % beta dot
    beta = (b(end,1)); % beta


    beta_save(:,count) = beta *(180/pi);
    betadot_save(:,count) = beta_dot *(180/pi);
indice = rev - (rev*360/tot_deg);
cc = beta_save(:, (indice):(rev));
ff = fft(cc);
P2 = abs(ff/(length(cc)));
P1 = P2(:,1:(length(cc))/2+1);
P1(:,2:end-1) = 2*P1(:,2:end-1);
beta_1s = P1(:,2);
beta_1c = P1(:,3);


dtt = trapz(dthrust_save);
dtt_save (:,count) = dtt;


dpii = trapz(dPi_save);
dpoo = trapz(dPo_save);
```

```
dp = dpii+dpoo;

dp_save (:,count) = dp;


ddrag = trapz(dcd_save);

ddrag_save (:,count) = ddrag;


end


end


Power = Nb*trapz(dp_save)*dpsi/ (2*pi);

Thrust = Nb*trapz(dtt_save)*dpsi /(2*pi);

Drag = Nb*trapz(ddrag_save)*dpsi /(2*pi)


Cpmr = Power/rho*pi*R*R*Vtip^3;

flat_area = 0.01

Cpp = 0.5*flat_area*advance^3;

Cp = Cpmr + Cpp;

Total_power = Cp*rho*pi*R*R*Vtip^3 /550; %hp


Ctmr = Thrust/rho*Vtip^2 *pi*R*R;
```

```
Ch = Drag/Vinf*Vinf*rho*pi*R*R ;


% Plots
% figure(1)
% plot(angle_plot, beta_save)
% title('flap angle for initial beta = 0 ')
% xlabel('psi (degrees)')
% ylabel('beta (deg)')
% axis ([0 360 0 10])
% xticks([0 90 180 270 360])


% figure(2)
% plot(r1, delta_ct_dr1)
% title('dct/dr vs r')
% xlabel('r')
% ylabel('dct/dr')
%
% figure(3)
% plot(r1, Cl1)
% %axis([0 1 0 2])
% title('Cl vs r')
% xlabel('r')
```

```
% ylabel('Cl')
%
% figure(4)
% plot(r1,lamda1)
% %axis([0 1 0 0.1])
% title('Inflow vs r')
% xlabel('r')
% ylabel('lambda')


%figure(2)
%plot(P1)
```

B. Flapping Function Code

```
function dydt= flap(tt,yy)
% function to solve flap equation
% y1 = beta
% y2 = beta_dot

load('Main_code.mat')

vb1 = evalin('base','vb');
lock1 = evalin('base', 'lock' );
mb1 = evalin('base','mb');

dydt = [yy(2); ((lock1 * mb1) - vb1*vb1*yy(1))];
```